Developmental Genetics of mouse mutant mesenchymal dysplasia (*mes*)

by Shigeru Makino

Doctor of Philosophy

Department of Genetics

School of Life Science

The Graduate University for Advanced Studies

1999

CONTENTS

CHAPTER I Abstract 1

CHAPTER II Introduction 5

CHAPTER III Identification of the causative gene for *mes* mutation 11

1. Introduction 11

2. Materials and methods 13

3. Results 16

3.1 Fine chromosomal location of *mes* 16

3.2 Molecular characterization of *ptc* gene in *mes* mutant 17

3.3 Allelism test of *mes* for *ptc* 18

4. Discussion 20

4.1 Linkage analysis of *mes* and other candidate genes 20

4.2 Molecular structure of *mes* Ptc protein 20

4.3 Dose effect of *ptc* on mutant phenotype 22

CHAPTER IV Phenotype analysis of $ptc^{-/mes}$ embryos 24

1. Introduction 24

2. Materials and methods 28

3. Results 32

3.1 Neonatal lethality of $ptc^{-/mes}$ embryos 32

3.2 Abnormal lung development 32

3.3 Increased body weight 34

3.4 Limb development of $ptc^{-/mes}$ embryos 35

4. Discussion 38

4.1 Neonatal lethality of *ptc*$^{-/nes}$ mice

and abnormal lung development 38

4.2 Increased body size in *ptc*$^{-/nes}$ embryos 39

4.3 Function of *ptc* in limb development 39

CHAPTER V GENERAL DISCUSSION 44

ACKNOWLEDGEMENTS 47

REFERENCES 48

CHAPTER I Abstract

mesenchymal dysplasia (*mes*) is a recessive mouse mutation mapped to Chromosome 13. It exhibits aberrant growth of mesenchyme-derived tissues. The most striking features of the mutant are excess skin and increased musculature. In addition, the mutant mouse shows dysmorphology, including preaxial polydactyly of all four feet, shortened face, bifurcate sternum and shortened kinky tail. In this study, to determine the chromosomal location of *mes*, I carried out the phenotype mapping, using intersubspecific cross. Based on 241 backcross progeny, *mes* was mapped to a region flanked by two microsatellite markers, *D13Mit 318* and *D13Mit 187*, where *patched* (*ptc*) has been mapped.

In order to examine the possibility that *ptc* gene is a candidate for *mes* mutation, I investigated the nucleotide sequence of *ptc* in *mes* mutation. The result revealed a 32 bp-deletion in the C-terminal cytoplasmic domain of *ptc*. Ptc is a transmembrane receptor protein for the secreted protein Shh that is expressed in the organizing centers in developing embryo, such as notochord, floor plate, ZPA of limb buds and lung. It is well established that Shh mediates a key signaling for cell growth and differentiation in developing embryo. In the absence of Shh, Ptc represses activity of Smoothened (Smo) that is a seven-pass transmembrane protein and constitutively activates the downstream genes including *Gli* and *ptc*. In the presence of Shh, Ptc is antagonized by Shh and Smo becomes active, thus the down stream genes are transcribed. *ptc* is highly conserved from fruitfly to human, but the C-terminal cytoplasmic domains differ among each

species. They are classified into two groups by the difference in the size of the domain. Higher vertebrates, such as chick and mammals, have "long type" C-terminal domain, whereas lower vertebrates and invertebrates have "short type" C-terminal cytoplasmic domain. *ptc* in *mes* can be classified into "short type" *ptc*.

In order to clarify that *mes* is *ptc* mutation, I performed allelism test of *mes* for *ptc* knockout allele (*ptc*$^-$) (Goodrich et al., 1997). As a result, all of 37 progeny that has both *ptc*$^-$ and *mes* alleles exhibited severe polydactyly phenotype, although neither single *ptc*$^-$ heterozygotes nor *mes* heterozygotes exhibited visible phenotype. This result indicated that *mes* is an allele at *ptc* locus and that the C-terminal cytoplasmic domain of Ptc plays an indispensable role in antagonistic activity for Shh signaling in developing limb bud.

In early development, Shh signaling plays an essential role in determination of the ventral fate of neural tube. In later developmental stages, Shh signaling acts to determine the local polarity and cell proliferation in various organs. Embryos homozygous for the *ptc* knockout allele have open neural tube and die around 10 dpc, and except for enlargement of body size the heterozygotes rarely exhibit visible phenotype. The early embryonic lethality in homozygotes and its recessive phenotype have hampered the study of *ptc* functions in later stage of development. In this study, it appeared that *mes* is a hypomorphic allele for *ptc* and the compound heterozygotes (*ptc*$^-$$^{/mes}$) survived just after birth. Taking this advantage, I could analyze roles of *ptc* in later developmental stages.

ptc$^{-/mes}$ mice appeared to die soon after birth because of inability of breathing.

Histological analysis demonstrated that lung mesenchyme overgrowed after about 17.5 dpc, and resulted in aplasia of pulmonary alveoli, which possibly explains for the neonatal lethality of $ptc^{-/mes}$ mice. This phenotype was similar to that observed in the transgenic mouse in which *shh* gene was overexpressed around the tip of the epithelial endoderm (Bellusci et al., 1997b). Thus, the observation in this study directly proved that function of *ptc* is essential in mouse lung development, and that Shh signaling acts in positive regulation of mesenchymal cell growth in lung development.

Body weight of $ptc^{-/mes}$ mice was 38% heavier than that of control littermates at 18.5 dpc. I carried out detailed histological analysis, and found overgrowth of mesenchymal cells in the dorsal region surrounding the neural tube, aorta and oesophagus. There was no significant alteration of *shh* expression pattern in 11.5 dpc $ptc^{-/mes}$ embryos when compared with the control littermates. It is likely that dorsal mesenchymal cells in $ptc^{-/mes}$ embryos overgrow at a long distance from *shh* expressing cells, probably in the absence of Shh protein. As previously described (Milenkovic et al., 1999), level of *ptc* activity possibly determines body size in a dose dependent manner. This study supported that *ptc* negatively regulates mesenchymal cell growth probably independent of Shh.

In mice, many preaxial polydactyly mutants show ectopic expression of *shh* and the zone of polarizing activity (ZPA) that provides organizing center activity at the posterior mesenchyme of the limb buds. Two mutants of them, Extra-toes (*Xt*) and Strong's luxoid (*lst*), are well characterized and the causative genes are identified to be transcription factors, *Gli3* and *Alx4*, respectively. These two genes are expressed at the

anterior mesenchyme of the limb bud, and are thought to repress potential expression of *shh* at anterior mesenchyme. Because $ptc^{-/mes}$ embryos exhibited preaxial polydactyly as severe as that of *Xt* and *lst*, I analyzed whether *shh* was ectopically expressed in $ptc^{-/mes}$ embryos. Indeed, *shh* was ectopically expressed at the anterior margin of the limb buds, but it was very weak, compared to other mutants. Expression of *shh* and *Fgf4* is interdependent and a positive feedback loop is established between the two genes. Hence, I analyzed *Fgf4* expression in developing limb buds of $ptc^{-/mes}$ embryos. The result indicated a very strong ectopic expression of *Fgf4* at the anterior apical ectodermal ridge (AER). It suggested that Shh signaling pathway to activate *Fgf4* transcription is sensitive to alteration or reduction of *ptc* activity in $ptc^{-/mes}$ embryos. On the other hand, intact activity of *Gli3* and *Alx4* genes, which repress potential *shh* expression, may account for the very low level of ectopic expression of *shh* at the anterior mesoderm in $ptc^{-/mes}$ limb buds. Thus, it is likely that the normal *ptc* expression at very low level in the anterior mesenchyme acts to prevent ectopic activation of Shh signaling.

In conclusion, this study revealed that *mes* is a mutation in the C-terminal cytoplasmic domain of Ptc protein that antagonizes Shh signaling. Using this unique mutant allele, I found that *ptc* play important roles in negative regulation of mesenchymal cell proliferation, alveoli formation in lung development and anteroposterior patterning of limb buds.

CHAPTER II Introduction

Morphogenesis in developing embryos is responsible for bringing cell population together for new inductive interactions and for building complex three-dimensional structures, such as hairs, lungs, limbs, eyes and so forth (Hogan, 1999). These organs are initially formed out of a simple epithelial sheet and mesenchyamal cell mass following determination of the whole body axes. In this process, signaling centers that arise in the organ primordia or specified positions determined by the original embryonic body axes play essential roles in cell growth and differentiation. The cell groups that constitute the signaling centers secrete intercellular signaling molecules, and the fate of surrounding cells that receive the molecule is determined. These molecules include fibroblast growth factors (FGFs), Bone morphogenetic proteins (BMPs), Hedgehogs and WNTs.

Sonic Hedgehog (Shh), one of mouse homologs of *Drosophila* Hedgehog (Hh), is produced in several tissues with organizing properties, including notochord, the floor plate and zone of polarizing activity (ZPA) of limb buds (Echelard et al., 1993; Riddle et al., 1993). Furthermore, Shh is predominantly expressed in epithelia at numerous sites of epithelial-mesenchymal interactions, including the tooth, hair follicle, gut and lung (Bitgood and McMahon, 1995). Both of *Drosophila* Hh and mouse Shh are produced as a precursor and are secreted outside the cells and undergoes autoproteolysis to generate an active N-terminal fragment (Lee et al., 1994; Porter et al., 1995, 1996a, 1996b). The autoprocessing reaction mediated by the C-terminal domain produces a

cholesterol-modified N-terminal fragment responsible for all known Hh/Shh signaling activity. This lipid-modified protein dramatically increases the hydrophobic property, and is tightly associated with the surface of the cells in which Hh/Shh is synthesized. The diffusion of the N-terminal fragment is spatially restricted and results in local high concentration of the N-terminal fragment on the surface of the Hh/Shh expressing cells. Thus, it causes the gradient of Hh/Shh concentration around its producing cells.

patched (*ptc*) was originally identified as a segment polarity gene in *Drosophila* and a key component of the hedgehog signaling pathway (Hooper and Scott, 1989; Nakano et al., 1989). Sequence analysis indicated that Ptc is a transmembrane protein with a postulated structure similar to channels or transporter proteins. In the absence of Hh signal, Ptc represses transcription of multiple genes that are induced by the Hh signal, including *wingless* (*wg*), a member of the Wnt family of secreted proteins, *decapentaplegic* (*dpp*), a member of the TGF-β superfamily, and *ptc* itself. In the presence of Hh, this repressive activity of Ptc is antagonized by Hh and transcription of the downstream genes including *ptc* itself is activated (Ingham et al., 1991; Capdevila et al., 1994; Tabata and Kornberg, 1994). These genetic and sequence data indicated that Ptc is a constitutive active receptor for Hh, being specifically inactivated by binding of the Hh ligand.

Another segment polarity gene essential for Hh signaling is *smoothened* (*smo*) that encodes a seven-pass membrane protein with characteristics of G protein-coupled receptors (Alcedo et al., 1996; van den Heuvel and P. W. Ingham, 1996). Because the phenotype of *Drosophila smo* mutant embryos is similar to that of *hh*, Smo was initially

thought to be a candidate for the receptor of Hh. However, there were two lines of evidence against this possibility. First, *smo* is epistatic to *ptc*, since in *ptc smo* double mutants, expression of the downstream genes disappears just as single *smo* mutant embryos. *ptc* is epistatic to *hh*, hence, *smo* is epistatic to *hh* and is negatively regulated by *ptc*. Second, Smo has functions independent of Hh. Although *ptc smo* double mutant does not express the downstream genes, *hh ptc* double mutant does (Alcedo et al., 1996; Hooper, 1994; Hammerschmidt et al., 1997). These genetic data indicated that Smo is a constitutive active signal transducer and is negatively regulated by Ptc in the absence of Hh ligand. In presence of Hh, Ptc is inactivated by binding of Hh and Smo becomes active.

This model initially proposed from the genetic data was subsequently investigated biochemically, using a mammalian Hh homolog Shh, Ptc and Smo (Stone et al., 1996). In those studies, Ptc could form a physical complex with Smo and bind Shh with high affinity, but Smo never bound Shh directly. This data, combined with genetic data from *Drosophila*, suggested that Ptc is a receptor for Shh, and Smo is a constitutive active signaling component that is repressed by Ptc in the absence of Shh.

Recent studies showed that some human diseases are associated with misregulation of the genes in Shh signaling (Hahn et al., 1999). The nevoid basal cell carcinoma (Gorlin) syndrome (NBCCS) (MIM 109400) is an autosomal dominant disorder with diverse phenotypic abnormalities, including high incidence of tumors, such as basal cell carcinoma (BCC) and medulloblastomas, as well as developmental defects, such as rib and craniofacial alterations, polydactyly, syndactyly and spina bifida

(Gorlin, 1987). Heritable mutations in NBCCS and somatic mutations in BCC were identified in *ptc* and *smo* genes, which give loss of function or gain of function of the respective gene products (Gailani et al., 1996; Xie et al., 1998; Johnson et al., 1996; Hahn et al., 1996; Kallassy et al., 1997). Loss of function type mutations in *shh* has been found in a fraction of familial cases of holoprosencephaly (HPE), which has a developmental defect of the midline structure of the forebrain and frequently the midface. In the most extreme cases, anophthalmia or cyclopia, and in the less severe form, ocular hypotelolism, defects of the upper lip and/or nose, and absence of the olfactory nerves or corpus callosum are observed (Roessler et al., 1996; Belloni et al., 1996). Furthermore, overexpression of *shh* in human skin or transgenic mice caused BCC (Oro et al., 1997; Fan et al., 1997), whereas loss of *ptc* function in mice also caused BCC and medulloblastoma at low frequency (Goodrich et al., 1997). These facts that Shh and Smo have positive effects and Ptc has negative effects in carcinogenesis are consistent with the model of Shh signaling in which Shh antagonizes the activity of Ptc, and Ptc negatively regulates the signal transducing Smo activity. Furthermore, loss of *shh* causes hypotelorism, whereas loss of *ptc* causes hypertelorism in developing mammalian embryos. This supports that Ptc plays roles in axial formation of developing embryo, in addition to Shh signal transduction.

The function of Ptc has been experimentally established from the use of *ptc* knockout mutant allele (*ptc*$^-$) that was produced by gene targeting. The homozygotes of the mutation are early embryonic lethal around 10 dpc, and its heterozygotes have almost normal phenotype except for slight enlargement of the body size. Consequently,

experimental study of the detailed functions of *ptc* in morphogenesis in later developing stages, especially in organogenesis process has been hampered by the property of the *ptc* null mutation.

In this study, I analyzed a mouse mutant, mesenchymal dysplasia (*mes*). *mes* is a recessive mouse mutation on Chr. 13 (Sweet et al., 1996), and exhibits aberrant growth of mesenchyme-derived tissues. The most striking features of the mutant are excess skin and increased musculature. In addition, the mutant mice have preaxial polydactyly of all four feet, a shortened face, wide set eyes, domened head and a shortened kinky tail. These phenotypes suggest that *mes* is a mutation which causes aberrant growth regulation of cells and/or the body axial formation like *ptc* mutant mice.

To determine the chromosomal location of *mes* and to identify the causative gene for *mes*, first I carried out linkage analysis by intersubspecific cross of the mutant mice with MSM strain that was derived from Japanese subspecific mouse, *Mus musculus molossinus*. As a result, *mes* appeared to be tightly linked to *ptc*. Subsequent sequencing analysis demonstrated that *mes* has a 32 bp-deletion in the coding region of the C-terminal cytoplasmic domain of *ptc* gene. In order to examine whether *mes* is an allele at *ptc* locus, allelism test was performed using the *ptc* knockout allele, *ptc*$^{-}$. Among the mice generated from the cross of the two mutants, the progeny which had both alleles of the *ptc* knockout mutation and *mes* exhibited preaxial polydactyly resembling to *mes* homozygotes but much severer than *mes* homozygotes. Since each single heterozygous mice rarely exhibit preaxial polydactyly, the result revealed that *mes* is allelic to the *ptc* knockout mutation, and the phenotype of *mes* is attributable to a

32 bp-deletion in the C-terminal cytoplasmic domain of *ptc*.

To investigate the functions of *ptc* in organogenesis more in detail, I analyzed the phenotype of compound heterozygotes the *ptc* knockout and *mes* alleles. First, I found that a large fraction of the compound heterozygotes died soon after birth because of their abnormal lung development, which is probably due to hyperplasia of mesenchymal cells in developing lung. It appeared that this overgrowth of mesenchymal cells prevented alveoli formation, which resulted in breathing problem. Second, body weight of the compound heterozygous embryos was larger than those of the control littermates. In combined with the phenotype in lung mesenchymal cells, these findings suggested that *ptc* acts as a negative regulator of proliferation of mesenchymal cells.

Finally, I analyzed the function of *ptc* in development of limb. *in situ* hybridization of the compound heterozygous embryos revealed very weak ectopic expression of *shh* at the anterior margin of the limb buds and strong ectopic expression of *Fgf4* in the anterior side of the AER. This result indicated that Ptc has function to repress *Fgf4* expression that is potentially activated by Shh signaling at the anterior margin of the limb buds.

Thus, this study demonstrated that *mes* is hypomorphic allele of *ptc* gene and that the C-terminal cytoplasmic domain of Ptc protein has an indispensable function to regulate proliferation of mesenchymal cells in mouse embryogenesis, especially in later stages of lung and limb development.

CHAPTER III Identification of the causative gene for *mes* mutation

1. Introduction

A number of mouse mutations with phenotype of preaxial polydactyly have been reported and genetically mapped. Among them, a recessive mutation mesenchymal dysplasia (*mes*) is mapped to Chromosome13 (Sweet et al., 1996). *mes* originally arose in the inbred strain CBA and have been maintained in the hybrid background of B6C3Fe-a/a strain. The mutation exhibits multiple skeletal anomalies, including preaxial polydactyly of all four feet, shortened face, wide set eyes, domened head and shortened kinky tail. The thoratic region is broader than that of normal mice and abnormal shaped sternum is observed. Excess skin and increased musculature in the shoulders and the hips are characteristic to the mutation. Some affected males are infertile because of a failure of the testis to descend, and females become pregnant but fail to deliver viable offspring. Because these abnormalities result from the malformations in mesoderm-derived cells, it has been thought that the wild-type *mes* acts as a growth regulator of mesenchymal cells during development and/or a factor involved in axial formation during development.

Recently, function of *patched* (*ptc*) gene, which is mapped to the mouse Chromosome 13, has been well documented. The gene product Ptc is known to be a transmenbrane receptor protein for a secreted protein Shh (Goodrich et al., 1996; Stone et al., 1996). It is suggested that developmental function of *ptc* is to repress the transmission of Shh signaling.

From the aspects of its chromosomal location, postulated function and mutant phenotype, *ptc* was thought to be a potential candidate gene for the *mes* mutation. In this chapter, to determine the fine chromosomal location of the *mes* gene, I carried out a linkage analysis of *mes* based on intersubspecific backcross. As a result, *mes* was mapped to a region flanked by two microsatellite markers, *D13Mit318* and *D13Mit187*, where *ptc* was mapped as well. Consequently, I examined whether *ptc* is the causative gene for *mes*. To do this, I analyzed the *ptc* gene of *mes* mutant. Sequence analysis demonstrated that *mes* has a 32 bp-deletion in the last cytoplasmic domain of *ptc*.

In order to confirm that the phenotype of *mes* is caused by this deletion, allelism test was further performed. Although heterozygotes of neither *mes* nor *ptc*$^{-}$ exhibited preaxial polydactyly, all progeny that has both *mes* and *ptc*$^{-}$ alleles exhibited much severe preaxial polydactyly than *mes* homozygotes. These results proved that *mes* is a mutation at *ptc* locus and that the phenotype of *mes* mutation is attributable to the 32 bp-deletion in the C-terminal cytoplasmic domain of *ptc*.

2. Material and method

Mice

C57BL/6, B6C3Fe-a/a-*mes*/+ (Sweet et al., 1996) and B6,129-*Ptch*^{tm1Mps} (Goodrich et al., 1997) were purchased from the Jackson Laboratory (Bar Harbor, Ma., USA). C57BL/6J-*mes*/+ was made by backcrossing of B6C3Fe-a/a-*mes*/+ to C57BL/6J for three or four generations in this study, and was used except linkage analysis. B6,129-*Ptch*^{tm1Mps} was also backcrossed to C57BL/6J for one or two generations. MSM strain was established at the National Institute of Genetics (NIG) and was derived from the Japanese wild mouse, *Mus musculus molossinus*. All these mice were maintained at NIG.

PCR genotyping

Genomic DNA for genotyping was prepared from ear, liver, tail, or amnion of embryos. The oligonucleotide primer pair to detect the deletion site of *ptc* in *mes* mutation were as follows: mesdF, 5'-TCCAAGTGTCGTCCGGTTTG-3' and mesdR, 5'-GTGGCTTCCACAATCACTTG-3'. Because the neomycin resistance gene is inserted in the *ptc* locus of B6,129 -*Ptch*^{tm1Mps}, the heterozygous mutant mice could be easily distinguished from the wild-type mice by presence of the neomycin resistance gene. The oligonucleotide primer pair to detect the transgene in the knockout mutant mice were as follows: neoP1, 5'-GGCTATTCGGCTATGACTGG-3' and neoP2, 5'-GAGATGACAGGAGATCCTGC-3'.

Linkage analysis

For linkage analysis of *mes*, (MSM x B6C3Fe-a/a-*mes/mes*)F1 mice were backcrossed to B6C3Fe-a/a-*mes/mes*. Since homozygous females fail to deliver viable offsprings (Sweet et al, 1996), only homozygous males were used. Genomic DNA was prepared from the liver or the ear of the backcross progeny. Microsatellite markers were purchased from Research Genetics (Huntsville, AL, USA). The PCR products were visualized by staining with ethidium bromide after separation on 3% agarose gel electrophoresis.

Southern blot analysis

Five micrograms of each genomic DNA from recombinant progeny were digested with *BamHI* or *HindIII*. DNA was separated on 1 % agarose gel electrophoresis and was blotted onto Hybond-N^+ nylon membrane (Amersham Pharmacia Biotech, Buckinghamshire, UK). A 841bp fragment of *ptc* 5'-coding region (Goodrich et al., 1996) was obtained from Dr. Matthew P. Scott. Hybridization was performed with ^{32}P-labeled *ptc* probe by a standard method (Sambrook et al., 1989). Autoradiographs were analyzed with BAS 2000 Bioimage Analyzer (Fuji Photo Film, Tokyo, Japan).

DNA sequence analysis

DNA sequence was determined for both strands by ABI 377 automated DNA sequencer (Perkin-Elmer Applied Biosystems, CT, USA), using BigDye Terminater Cycle

Sequencing FS Ready Reaction Kits (Perkin-Elmer Applied Biosystems, CT, USA).

Construction of mes cDNA library

Total RNA was extracted from 14.5 dpc *mes/mes* embryos, using RNeasy Mini Kits (QIAGEN) and contaminating DNA was digested by DNaseI (Boehringer Mannheim). The mRNA was purified from total RNA using QuickPrep Micro mRNA Purification Kits (Amersham Pharmacia Biotech, Uppsala, Sweden) and cDNA was synthesized from 5 ug of the mRNA with ZAP-cDNA Synthesis Kits (Stratagene, La Jolla, CA, USA). The cDNA ligated to Lambda ZAPII vector was packaged with Gigapack II Gold Packaging Extract (Stratagene, La Jolla, CA, USA).

Screening procedures and cDNA cloning

The cDNA library was screened by plaque hybridization with the ^{32}P-labeled 841bp DNA fragment of *ptc* 5'-coding region as a probe described above. Ten independent clones were isolated and two of them were further analyzed.

3. Result

3.1 Fine chromosomal location of *mes*

Determining chromosomal location of mutation is essential to search and identify the causative gene for the mutation. In this study, first I attempted to map *mes* mutation and carried out a linkage analysis for other known genes as potential candidates for *mes*. In this mating experiment, I crossed *mes* mutant mice with an inbred strain MSM, which was established from Japanese wild mice, *Mus musculus molossinus*, because a high level of simple sequence length polymorpholism (SSLP) of microsatellite markers was available between MSM and the *mes* mutant strain.

Because penetrance of polydactylous phenotype of *mes* was known to be high, all backcross progeny was used for the linkage analysis, and the progeny with preaxial polydactyly was typed as *mes* homozygotes. There was only one progeny that did not exhibit preaxial polydactyly but showed the typical phenotype of *mes*, such as the thickened feet and the shortened face. I dealt this progeny as a *mes* homozygote. Based on total 241 backcross progeny, *mes* was mapped to a 1.7 cM long interval flanked by two microsatellite markers, *D13Mit318* and *D13Mit187*. *mes* mutation was separated by one recombinant from the proximal marker *D13Mit318*, and separated by two recombinants from the distal marker *D163Mit187* (Fig. 1a, b).

There are several genes that have been mapped to this region of Chromosome 13. I searched the genes on a database, Encyclopedia, to test the possibility that they are potential candidates for *mes*. This analysis demonstrated that one of these genes, *patched* (*ptc*), was tightly linked and there was no recombinant between *mes* and *ptc*.

3.2 Molecular characterization of *ptc* gene in *mes* mutant

Previous studies suggested that *ptc* has two functions as a negative regulator of cell growth and a factor required for body axis formation. Homozygotes of *mes* exhibit thickened feet and excessive skin in possible consequence of hyperproliferation of cells, and they also have preaxial polydactyly in consequence of aberrant axis formation. Therefore, *ptc* seemed to be a good candidate gene for *mes*.

For characterization of *ptc* gene in *mes* mutant, I constructed a cDNA library from 14.5 dpc *mes* homozygous embryos and isolated ten independent cDNA clones by screening of the library with the *ptc* probe. Two of them were sequenced completely for their coding region. Comparison of the coding sequence of *mes* with that of a wild-type gene of C57BL/6 strain revealed that there was a 32-bp deletion in the coding sequence of the *mes* gene (Fig. 2a). To examine whether this deletion occurred in the genomic DNA of *mes* or it represented a splicing variation of the mRNA, I analyzed PCR-amplified DNA sequences from genomic DNAs of various mouse strains as templates with a primer pair flanking the deletion site in the *ptc* cDNA (Fig. 2b). Because *mes* arose in CBA strain and has been maintained in hybrid background of (C3H x C57BL/6)F1, the length of the PCR product of the *ptc* cDNA from *mes* should be identical to that of either CBA, C3H or C57BL/6J strain. I found that the PCR product from *mes* is smaller than that of other three strains (compare lane 4 with lane 1, 2 and 3 in Fig. 2b). Furthermore, the sequence of the PCR products of the *mes* cDNA clone was completely identical to that of the *mes* genomic DNA. All results demonstrated that the *ptc* gene of *mes* has a 32-bp deletion in the genomic DNA. This deletion causes a

frameshift mutation, adding aberrant 68 amino acids to the C-terminal cytoplasmic domain, following the deletion site (Fig. 4).

Ptc is a twelve-transmenbrane protein and constitutes a receptor complex for Sonic Hedgehog (Shh) in conjunction with Smoothened (Smo) protein. Ptc protein is highly conserved from fruitfly to mouse, but there are several divergent regions among different organisms. One of them is the C-terminal cytoplasmic domain. Fruitfly and fish have a short domain, whereas mouse, chick and human have a long domain (Fig. 3, 4, and 5). Nevertheless, amino acids of this C-terminal domain is highly conserved between mouse and human (about 71 % identity between the two species). Ptc of *mes* mutation lost most of the C-terminal cytoplasmic domain, which is conserved in chick and mammals. The phenotype of *mes* mutation appeared to be caused by the loss of functions of the C-terminal domain of Ptc protein.

3.3 Allelism test of *mes* for *ptc*

To confirm that *mes* is an allele at the *ptc* locus, allelism test was performed, using *ptc* knockout mutant allele, hereafter I designates as *ptc*$^-$, in which a part of *ptc* gene including the putative start codon was replaced by *lacZ* and a neomycin resistance gene (Goodrich et al., 1997). Both *mes* and *ptc*$^-$ are recessive mutations. Heterozygotes of *mes* never show any visible phenotype, likewise *ptc*$^-$ heterozygotes also rarely show preaxial polydactyly (only about 1% of heterozygotes exhibit polydactyly). If *mes* was allelic to *ptc*$^-$, mice that have both mutant alleles were expected to exhibit polydactyly like *mes* homozygotes. In this study, *mes* heterozygotes were crossed with *ptc*$^-$

heterozygotes, and the resultant progeny was investigated for the polydactyly phenotype (Fig. 6). All 37 embryos from 15.5 dpc to P0 (new born), which had both *mes* and *ptc*$^-$ alleles, showed preaxial polydactyly in all four feet, being severer than the phenotype of *mes* homozygotes. One of 53 embryos that had only *ptc*$^-$ allele showed polydactyly of only one foot. This phenotype was so weak that it was easily distinguishable from that of mice with both mutant alleles. The remaining 52 embryos had normal limbs. None of 62 progeny that had only *mes* allele and none of 58 progeny that had two wild-type alleles showed polydactyly. These results indicated that *mes* is an allele at the *ptc* locus, and the phenotype of *mes* mutation is attributable to the 32 bp-deletion of the C-terminal cytoplasmic domain of *ptc*.

4. Discussion

4.1 Linkage analysis of *mes* and other candidate genes

In this study, *mes* was mapped between *D13Mit318* and *D13Mit187*. Considering the putative functions of the *mes* gene, such as regulation of mesenchyme formation or mesodermal cell proliferation, two other genes, growth arrested specific gene 1 (*gas1*) and modifier of *Dac* (*mdac*), both of which mapped to the same chromosomal region, were potential candidates for *mes*. *gas1* was isolated as a gene preferentially expressed in growth arrested G0 cells (Schneider et al., 1988). Therefore, *gas1* might be involved in negative growth regulation of cells. *mdac* is a recessive polymorphic allele that may exist in several laboratory mouse strains (Chai, 1981). In the genetic background of *mdac* homozygote, phenotype of dominant limb mutation Dactilia (*Dac*), characterized by the absence of the three middle digits of all four feet, is expressed. Although I could not examine whether *mes* is genetically separated from these two genes, the present genetic data clearly excludes *gas1* as *mes* candidate. The possibility that *mdac* is allelic to *mes* (*ptc*) is not still excluded and remains as an open question.

4.2 Molecular structure of *mes* Ptc protein

At present, *ptc* homologs have been identified in fruitfly, zebrafish, chick, mouse and human (Nakano et al., 1989; Concordet et al., 1996; Marigo, et al., 1996a; Goodrich et al., 1996; Johnson et al., 1996). Furthermore, second *ptc* homolog, designated as *ptc2*, was identified in zebrafish, mouse and human (Motoyama et al., 1998; Carpenter et al., 1998). Ptc is a twelve transmembrane protein and is highly conserved from fruitfly to

human (Fig. 3). Mouse Ptc shared 35% and 96% identity with fruitfly and human Ptc, respectively. But there are two relatively divergent regions in amino acid sequence among various species. One is the region between putative transmembrane domain 6 and 7, representing a large cytoplasmic domain that may influence determination of the ligand specificity in each species. This domain of mouse Ptc, which includes 153 amino acids, shares 36 amino acids (24%) identity with that of fruitfly. The other divergent domain is the C-terminal cytoplasmic domain. This domain of mouse Ptc includes 273 amino acids, whereas fruitfly and fish Ptc have much shorter domains, consisting of 183 and 55 amino acids, respectively. Moreover, lower level of amino acid identity is also found in the remaining short stretch of the domain between mouse and two other species, fruitfly and fish. On the other hand, the C-terminal domain of mouse Ptc shares high identity with that of human (90 %) and chick (71 %) (Fig. 4).

It is notable that all Ptc2 proteins identified in different species has "short type" domain similar to Ptc protein of fruitfly and fish. Thus, members of Ptc protein can be classified into two groups, "long type" that are represented by Ptc of mouse, chick and human, and "short type" that are represented by Ptc of fruitfly and fish and Ptc2 (Fig. 5). It is likely that additional amino acids stretch was attached to the C-terminal cytoplasmic domain of "short type" Ptc protein during evolution of higher vertebrates, giving rise to "long type" Ptc.

In this study, I found a 32 bp-deletion in the C-terminal cytoplasmic domain of *ptc* in *mes* mutation. This deletion converted "long type" into "short type" type Ptc with the new aberrant 68 amino acids stretch in the C-terminal cytoplasmic domain. Stone et

al. (1996) reported that Ptc protein is physically associated with Shh and Smo, using Ptc that was truncated after amino acid 1293 and had an attached epitope tag to the C-terminal cytoplasmic domain (Fig. 4). They found that binding affinity of the truncated Ptc with Shh molecule is similar to that of full-length Ptc. *ptc* gene of *mes* is mutated at 1215 amino acid residue and the intact region of the C-terminal domain of *mes* was 79 amino acids shorter than Ptc protein used in Stone's experiment. If *mes* Ptc incorrectly interacts with Shh, the 79 amino acids region may be responsible for correct binding with Shh molecule. Alternatively, if *mes* Ptc correctly interacts with Shh, it is possible that the C-terminal domain of Ptc acts as a repression domain for Smo activity, and that *mes* Ptc can not completely repress the signal transmission by Smo. This malfunction of *mes* Ptc may result in constitutive activation of Smo, which is transferred to the downstream of the Shh signaling.

4.3 Dose effect of *ptc* on mutant phenotype

In this study, I clearly demonstrated that *mes* was allelic for ptc^-. In the allelism test cross, I found that there is a large variation in the severity of phenotype, depending on the combination of mutant alleles. As previously reported, the severest phenotype was observed in homozygotes of the knockout allele (ptc^-). The homozygous embryos died around 10 dpc (Goodrich et al., 1997). As shown in this study, the compound heterozygotes ($ptc^{-/mes}$) also showed very severe phenotype. Most of them died just after birth (see section IV) and exhibited severe preaxial polydactyly with high penetrance (37/37). When compared with these phenotypes, *mes* homozygotes exhibit rather milder

phenotype, such as preaxial polydactyly with high penetrance (115/116), and slight increase of the body size. *ptc*$^{-}$ heterozygotes showed further milder phenotype. They rarely exhibited preaxial polydactyly (3/389). In contrast to these *ptc* mutant phenotypes, mice which overexpress *ptc* show opposite phenotype, namely decreased body size (Milenkovic et al., 1999). All these findings suggested that mutant phenotype is determined by the levels of Ptc activity. Comparing with the *ptc* null mutation, *mes* still retains *ptc* activity to some extent. In this context, it is likely that *mes* is a *ptc* hypomorphic allele.

CHAPTER IV Phenotype analysis of *ptc*$^{-/mes}$ embryos

1. Introduction

In organogenesis of limb, branchyal arche, genitalia, feather and lung, budding morphogenesis is one of key processes to form their complex three-dimensional structure (Horgan, 1999). Among them, lung and limbs are best understood, as model systems to study the morphogenesis.

Lung development begins at 9.5 dpc. At this stage, forgut at the initiation region of elongation is surrounded by the splanchinic mesoderm (Hogan, 1999). Initially, *Bmp4* and *Fgf10* are expressed in the potential lung field of splanchinic mesoderm surrounding gut tube, and *shh* is expressed in the epithelium of ventral forgut (Weaver et al., 1999; Litingtung et al., 1998; Bellusci et al., 1997b). Because lung is not formed at all in *Fgf10* deficient mice, *Fgf10* is essential for the initiation of lung development (Sekine et al., 1999). In *shh* deficient mice, tracheoesophareal septum is not established, and trachea and esophagus are fused, indicating that the Dorsal-Ventral axis of forgut is not formed correctly. Although several genes, such as *shh* and *Fgf10*, were identified to be involved in lung morphogenesis, the detailed mechanism by which initiation of lung formation occurs is poorly understood.

In growing lung buds, *Fgf10* is expressed at the distal tips of the mesoderm. Proliferation of the epithelial endodermal cells are induced by *Fgf10*. The direction of gut elongation might be determined by *Fgf10*, considering the character of Fgf10 as a chemoattractant (Bellusci et al., 1997a; Park et al., 1998). *Bmp4* is highly expressed at

the distal tip of epithelial endoderm and in the adjacent mesenchyme. Over- and mis-expression of antagonizing factors demonstrated that *Bmb4* is essential for the endodermal cells to adopt the distal character of the lung (Bellusci et al., 1996; Weaver et al., 1999). *shh* is also expressed at the distal tip of epithelial endoderm and *ptc* is expressed in the distal mesenchyme. Since mesenchyme is poorly formed in *shh* deficient mice, and overexpression of *shh* at the distal endoderm results in overgrowth of the mesenchyme, Shh signal is thought to act as a positive growth regulator in the distal mesenchyme (Litingtung et al., 1998; Bellusci et al., 1997b). With elongation of terminal end buds, branching of bronchioles occurs repeatedly, and pulmonary tree is generated. By 17.5 dpc, the cells of proximal and distal endoderm can be distinguished by their morphological characters. The proximal endodermal cell of bronchioles is columnar and ciliated, whereas the distal one is low cuboidal or squamous.

At birth, lung is filled with air and expands. Terminal differentiation of the distal endodermal cells into type I (squamous) and type II (cuboidal) pneumocytes occurs after birth. Distal epithelial sacs are further divided into alveoli by secondary septation. By this later process, the surface area of lung increases. As mentioned above, epithelial-endodermal interaction is very important in lung development.

Limb development begins with a restriction of *Fgf10* expression domain in the lateral plate mesoderm, which is initially expressed widely in entire lateral plate mesoderm (Ohuchi et al., 1997). *Fgf10* deficient mice exhibit complete loss of fore and hind limbs (Sekine et al., 1999). The restriction of *Fgf10* expression induces expression of *Fgf8* in the presumptive limb field of overlying ectoderm, and limb formation is

initiated. Once limb bud is formed, outgrowth of the limb bud depends on both apical ectodermal ridge (AER) and zone of polarizing activity (ZPA). AER is a specialized epithelial structure that can be visibly distinguished from other ectodermal cells, and can be substituted by Fgf4 (Laufer et al., 1994; Niswander et al., 1994). AER supplies cell growth signals including Fgf4 to progress zone (PZ) which consists of undifferentiated mesenchymal cells subjacent to AER. The signals likely specifies PZ cells to their fates along proximal-distal axis. A molecule mediating the ZPA activity is known to be Shh protein. When ZPA is implanted at anterior mesenchyme of limb buds, anterior ectopic digits are formed. It is also seen when *shh* is overexpressed or Shh-soaked bead is implanted. (Riddle et al., 1993; Laufer et al., 1994; Lopez-Martinez et al., 1995). Expression of *Fgf4* in AER and *shh* in ZPA are interdependent (Laufer et al., 1994; Niswander et al., 1994). Removal of AER results in disappearance of *shh* expression and removal of ZPA results in disappearance of *Fgf4* expression. In addition, ectopic application of Shh results in ectopic expression of *Fgf4* at the anterior AER, and both ectopic expression of *Fgf4* and application of retinoic acid (RA) result in ectopic *shh* expression at the anterior mesenchyme. In other words, *shh* is necessary and sufficient for expression of *Fgf4*, and *Fgf4* maintains expression of *shh*. Although it is unknown whether RA indeed has some role in a living body, in above situation RA is thought to be a trigger for the initiation of *shh* expression.

In mice, many mutants that exhibit preaxial polydactyly are known. They are; Extra-toes (*Xt*), Strong's luxoid (*lst*), Recombination induced mutant 4 (*Rim4*), Hemimelic extra toes (*Hx*) and X-linked polydactyly (*Xpl*). Among these mutants, the

causative genes were identified in the former two mutants, but not in the others. Xt^J has a large deletion in a transcription factor gene *Gli3*, and lst^D has a 16-bp deletion in the homeobox domain of another transcription gene *Alx4*. Both are thought to be loss of function-type mutation. In these two mutants, ectopic expression of *shh* at the anterior margin of the limb buds is observed, which results in the duplication of the anterior digits (Masuya et al., 1995, 1997; Qu et al., 1997). Because disruption of *Gli3* or *Alx4*, which is normally expressed at the anterior mesenchyme, results in ectopic expression of *shh*, the normal function of these two genes is thought to repress potential expression of *shh* at anterior margin of the limb buds. The mechanism of the repression of *shh* at anterior mesenchyme, however, is unknown, and the mechanism by which *shh* is expreseed only at posterior mesenchyme in normal development is also poorly understood.

As mentioned above, Shh signaling is essential in both lung and limb development. Because embryo with *ptc* null mutation by gene targeting is lethal at an earlier developmental stage, roles of Shh signaling in lung and limb development, especially at the later organogenesis stage is not still clear. Embryos of the compound heterozygotes of ptc^- and *mes* alleles, $ptc^{-/mes}$, survive till just after birth. This allowed the analysis of the roles of Ptc and Shh signaling pathway even at later embryonic stages. In this chapter, I investigated the phenotype of $ptc^{-/mes}$ embryos more in detail. I found that lung and limb of the $ptc^{-/mes}$ embryos were severely affected. This result indicated that *ptc* has an important role in epithelial-mesenchymal interaction in development of these two organs.

2. Materials and methods

Whole mount in situ hybridization

Whole mount *in situ* hybridization was performed following the method of Prince and Lumsden (1994), with some modifications. Embryos were fixed overnight at 4°C in 4% PFA-PBS, washed twice in PBS containing 0.1% Tween20 (PBT), and then dehydrated through a series of ethanol (25%, 50%, 75% and 100%) in PBT. Following successive rehydration, embryos were treated with 20 ug/ml ProteinaseK (Boehringer Mannheim) for 30 minutes and then incubated in 2 mg/ml glycine/ PBT for 5 minutes to stop the reaction of ProteinaseK. After washed twice, embryos were postfixed in 0.2 % glutaraldehyde/4% PFA-PBS at room temperature and washed twice. Following the incubation in PBT at 70°C for 30 minutes, embryos were incubated in 6% H_2O_2/ PBT at room temperature for 1 hour. After 3 times PBT washes, the embryos were prehybridized in hybidization buffer (50 % formamide, 5 x SSC (pH 5.0), 1 % SDS, 50 ug/ml yeast tRNA, 50 ug/ml heparin) for 1 hour at 70°C. Embryos were hybridized overnight in prehybridization buffer containing a digoxygenin-labelled RNA probe (0.3 ug/ml). RNA probes were synthesized according to the manufacture's instructions (Boehringer Mannheim). Embryos hybridized with the probes were washed three times for 30 minutes with solution I (50 % formamide, 1 % SDS, 5 x SSC (pH 4.5)) at 70°C, and followed by wash in RNase buffer (0.5 M NaCl, 10 mM Tris-HCl (pH 7.5), 0.1 % Tween20). Embryos were treated with 100 ug/ml RNaseA for 30 minutes at 37°C, and washed twice with solution II (50 % formamide, 2 x SSC (pH 4.5)) for 30 minutes each

at 65°C, and washed in Tris-buffered saline containing 0.1 % Tween20 (TBST). Embryos were preblocked in 1.5% Blocking reagent (Boehringer Mannheim) in TBST before being incubated overnight in antibody solution at 4°C. To prevent nonspecific binding of antibody, alkaline phosphatase conjugated anti-digoxigenin antibody (Boehringer Mannheim) was pre-absorbed with mouse embryo powder. The embryos were washed extensively in TBST. The coloring reactions were performed in BM purple AP substrate (Boehringer Mannheim). Stained embryos were viewed under dissection microscopy.

Section in situ hybridization

Section *in situ* hybridization was performed following the method of Birren et al. (1993), with some modifications. Embryos were fixed for 6 hours at room temperature in 4% PFA-PBS, replaced in PBS containing 30 % sucrose for overnight at 4°C. Embryos were embedded in OCT compound (Sakura Finetechnical Co. Ltd., Tokyo, Japan) and frozen in liquid nitrogen. Sections were cut with 25 um thickness and dried at 37°C for 2 hours, refixed in 4% PFA-PBS for 20 minutes at room temperature. Following washing twice in PBS, sections were treated for 2 minutes in PK buffer (50 mM Tris-HCl (pH 7.5), 5 mM EDTA, 50 ug/ml Proteinase K) at room temperature, washed twice in PBS, and fixed in 4% PFA-PBS for 5 minutes at room temperature. Following washing in water, sections were put in 0.1 M triethanolamine-HCl (pH 8.0) (TEA), and stirred for 2 minutes. Acetic anhydride was added to TEA at one four hundredth volume, and sections were left for 10 minutes and washed in PBS and 0.85 % NaCl. Sections

were prehybridized at 60°C in prehybridization buffer (50 % formamide, 1 mg/ml yeast tRNA, 100 ug/ml heparin, 1 x Denhardt's solution, 0.1 % Tween20, 0.1 % CHAPS, 5 mM EDTA), and after one hour sections were hybridized in prehybridization buffer containing 1-2 ug/ml probe at 60°C. After hybridization for overnight, sections were washed for 10 minitues in 1 x SSC, 0.3 % CHAPS at 60°C, and 10 minutes in 1.5 x SSC, 0.3 % CHAPS at 60°C, and cool down to 37°C. Sections were further washed twice for 20 minutes in 2 x SSC, 0.3 % CHAPS at 37°C, and 30 minutes in 2 x SSC, 0.3 % CHAPS, 20 ug/ml RnaseA at 37°C, and twice for 10 minutes in 2 x SSC, 0.3 % CHAPS at room temperature. Sections were then washed for 30 minutes in 0.2 x SSC, 0.3 % CHAPS at 60°C, and twice for 10 minutes in 0.1 % Tween20, 0.3 % CHAPS / PBS at 60°C. After washing for 10 minutes in 0.1 % Tween20 in PBS at room temperature, and 10 minutes in PBT (2 mg/ml BSA, 0.1 % Triton-X100 in PBS) at room temperature, sections were preblocked in 20 % sheep serum in PBT before being incubated overnight in antibody solution at 4°C. The same antibody as described in whole mount hybridization was used. Following four times wash in PBT at room temperature, twice in alkaline phosphatase buffer (100 mM Tris-HCl (pH 9.5), 100 mM NaCl, 0.1 % Tween20, 50 mM $MgCl_2$, 5 mM levamisole), sections were stained for 2 hours to overnight in staining solution (75 mg/ml NBT, 50 mg/ml BCIP in alkaline phosphatase buffer) at room temperature. When slides were stained properly, slides were fixed in MEMFA (100 mM MOPS (pH 7.5), 1 mM $MgSO_4$, 2 mM EGTA, 3.7 % formaldehyde) at room temperature for 2 hours, and mounted with 50 % glycerol.

X-gal staining of embryos

Embryos were fixed for 10 minutes in 4% PFA-PBS at room temperature, and washed twice in PBS (pH 7.5). Staining reaction was performed in staining solution (0.2 mM $K_3Fe(CN)_6$, 0,2 mM $K_4Fe(CN)_6$, 2mM $MgCl_2$, 1 mg/ml X-gal, PBS (pH 7.5)) at 37°C .

Probes

The following probes were used in *in situ* hybridization studies: *shh* (Echelard et al., 1993), *pax1* (Deutsch et al., 1988) and a 1.3 kb *Bmp4* cDNA fragment were provided by Dr. A. McMahon, Dr. U. Deutsch and Dr. Y. Takahashi, respectively.

Skeletal staining

Embryos at 18.5 dpc and several days old mice were used for analysis of skeletal phenotype. Embryos and mice were prefixed in 70% ethanol overnight. After the skin and viscera were removed, they were fixed in 95% ethanol and subjected to enough treatment with acetone. Then they were stained for 1 weeks with 0.01 % Alcian blue and 0.1 % Alizalin red in 5 % acetic acid at 37°C. Finally the skeletons were cleared by 2 % KOH, following several washes with water, and then transferred into glycerol.

3. Results

3.1 Neonatal lethality of *ptc*$^{-/mes}$ embryos

As I stated in the Chapter III, no viable progeny of *ptc*$^{-/mes}$ was obtained from the allelism test cross. This suggested that the *ptc*$^{-/mes}$ embryos die before or just after birth. In order to determine when the *ptc*$^{-/mes}$ embryos die, *ptc*$^{-}$ heterozygotes were mated with *ptc*^{mes} heterozygotes, and the genotypes of the embryos generated from the cross were analyzed in different developmental stages (Table 1). As a result, embryos with each of four genotypes were observed approximately in the Mendelian segregation ratio until 18.5 dpc, although a small fraction of *ptc*$^{-/mes}$ embryos had already been dead. For example, 2 embryos were dead at 18.5 dpc. They exhibited enlarged body size and hyperplasia and/or hypertrophy of the skin or mesenchyme under the skin. Some other viable *ptc*$^{-/mes}$ embryos also exhibited similar phenotype (Fig. 7).

At birth, I obtained a total of 34 viable progeny that were genotyped as either of *ptc*$^{-/+}$, *ptc*$^{+/mes}$ and *ptc*$^{+/+}$, but I had only one viable and two dead progeny of *ptc*$^{-/mes}$. This viable mouse looked pale, like cyanosis. Histological analysis revealed that the mouse had malformation of lung, because of mesenchymal hyperproliferation (see bellow). The result suggested that most of *ptc*$^{-/mes}$ embryos did not die in utero, but died after birth, because of breathing problem.

3.2 Abnormal lung development

New born mice of the *ptc*$^{-/mes}$ die soon after birth, probably due to inability of breathing. Macroscopic observation of the lung of 16.5 dpc *ptc*$^{-/mes}$ embryos revealed no significant

abnormalities, in comparison with the control littermates (Fig. 8a, b). At 18.5 dpc, the lung of $ptc^{-/mes}$ embryos tended to be smaller and was not sufficiently spread. Lines of the bronchiole were not seen under strong light at the apical site of $ptc^{-/mes}$ lung (Fig. 8c, d). At birth, $ptc^{-/mes}$ lung became much smaller than that of the control embryos. To study the abnormalities of the lung in $ptc^{-/mes}$ embryos more in detail, I carried out a histological analysis of embryos from 16.5 dpc to birth (Fig. 9). Consistent with the macroscopic observation, the section of $ptc^{-/mes}$ lung at 16.5 dpc showed no significant difference from that of $ptc^{+/+}$ embryos. At 17.5 dpc, epithelial sac-like structure, which become alveoli in future, was observed in both $ptc^{+/+}$ and $ptc^{-/mes}$ lungs, but this structure of the $ptc^{-/mes}$ lung was comparatively smaller. The mesenchymal cells of $ptc^{-/mes}$ lung tended to overgrow. At 18.5 dpc, the airway of $ptc^{-/mes}$ lung was much thinner than that of $ptc^{+/+}$ embryo, but the columnar cells in the proximal part and the cuboidal or squamous cells in the distal part in $ptc^{-/mes}$ were easily distinguished from each other (Fig. 9e, f and Fig. 10). It was notable that the mesenchymal cells of $ptc^{-/mes}$ lung further overgrew. In new born $ptc^{+/+}$ mice, many alveoli were formed in their lung and the alveoli contained air and expanded. In contrast, alveoli were not formed in the new born $ptc^{-/mes}$ mice. The absence of alveoli, which is normally filled with air, is likely to be responsible for the smaller size of $ptc^{-/mes}$ lung at macroscopic level.

To examine whether Proximal-Distal (P-D) axis formation is affected in the lung of $ptc^{-/mes}$, section *in situ* hybridization was performed (Fig. 11). The level or domain of *Bmp4* expression in 15.5 dpc $ptc^{-/mes}$ embryos was similar to that in the lung of $ptc^{+/+}$embryos. In addition, I found that morphology of endodermal cells in $ptc^{-/mes}$

lung was normal. Altogether, the P-D axis formation of the $ptc^{-/mes}$ lung was not affected, and abnormality of $ptc^{-/mes}$ lung is likely to be restricted to the hyperplasia of the mesenchymal cells.

3.3 Increased body weight

Increased body weight caused by *ptc* mutations is a common character in human and mouse (Goodrich et al., 1997; Hahn et al., 1998; Milenkovic et al., 1999). Hence, I analyzed the body weight of 18.5 dpc embryos obtained from the same cross as was used in the allelism test of *mes*. I found that $ptc^{-/mes}$, $ptc^{-/+}$ and $ptc^{+/mes}$ embryos were 38%, 21% and 10% heavier than the $ptc^{+/+}$ littermates, respectively (Fig. 12). The result suggested that normal *ptc* gene negatively regulates body size in dose dependent manner.

Hematoxylin and eosin stained sections of $ptc^{-/mes}$ embryos at 13.5 dpc showed that mesenchyme of the trunk overgrew around the neural tube, esophagus and aorta, especially under the dorsal skin (Fig. 13a, b). Sclerotome derives from the ventromedial somite and is thought to be directly induced by Shh (Johnson et al., 1994; Fan and Tessier-Lavigne, 1994). In later development, sclerotomal cells migrate and differentiate into skeletal elements, including vertebral column and ribs. To examine whether the overgrown mesenchymal cells in $ptc^{-/mes}$ embryos were derived from the sclerotome, expression of a sclerotomal marker *Pax1*, was analyzed for the $ptc^{-/mes}$ embryos. Section *in situ* hybridization of the $ptc^{-/mes}$ embryos at 11.5 dpc demonstrated no significant alteration of the *Pax1* expression domain (Fig. 13e, f). This observation

indicated that the overgrowing mesenchymal cells in the trunk are not descendant cells that had migrated from the sclerotome.

Subsequently, I examined the expression of *shh* in $ptc^{-/mes}$ embryos at 11.5 dpc. I found no significant alteration of *shh* expression pattern in the notochord and the floor plate, and no ectopic expression of *shh* in the dorsal trunk (Fig. 13c, d). Thus, it appeared that hyperplasia of the mesenchymal cells in $ptc^{-/mes}$ embryos is not due to ectopic expression or upregulation of *shh*. The results also suggested that Ptc protein has roles in negative growth regulation of mesenchymal cells that do not receive Shh in the normal condition. In this context, Ptc protein may not act as a receptor for Shh, but a simple repressor of mesenchymal cell growth, because Shh generated in the notochord and the floor plate can not migrate to the dorsal regions across such a long distance.

3. 4 Limb development of $ptc^{-/mes}$ embryos

All $ptc^{-/mes}$ mice examined in this study exhibited preaxial polydactyly, typically 7 digits, being more severe than the phenotype of $ptc^{mes/mes}$ mice, which is characterized by 6 digits (Fig. 14). Many other preaxial polydactyly mutants showed ectopic *shh* expression at the anterior margin of the limb buds. To address the question whether *shh* is also ectopically expressed at the anterior margin of the limb buds in $ptc^{-/mes}$ embryos, I carried out whole mount *in situ* hybridization analysis of 11.5 dpc $ptc^{-/mes}$ embryos with *shh* cRNA as a probe. As shown in Fig. 15, in $ptc^{+/+}$ embryos *shh* was expressed strongly and exclusively at the posterior margin of the both fore- and hindlimb buds. In one of two $ptc^{-/mes}$ embryos, *shh* was ectopically expressed at the anterior margin of both

hindlimb buds in addition to the normal posterior expression (Fig. 15b, arrowhead). This ectopic expression was very weak when compared with that of other preaxial polydactyly mutants, such as *Xt*, *lst*, and *Rim4*. Furthermore, ectopic expression of *shh* was not detected in the forelimb buds, even though all of the $ptc^{-/mes}$ embryos exhibited preaxial polydactyly in all four feet as severe as other mouse mutants.

It was reported that ectopic *shh* at anterior mesoderm of limb buds induces ectopic expression of *Fgf4* at anterior AER. I analyzed expression of *Fgf4* in the limb buds of the $ptc^{-/mes}$ embryos at 11.5 dpc (Fig. 15c-f). As a result, ectopic *Fgf4* expression was detected at the anterior AER of the both fore- and hindlimb buds in the $ptc^{-/mes}$ embryos, and the expression domain was fused to the normal expression domain at posterior two third of limb buds. This ectopic expression was very strong through whole AER, and was detected in all four feet.

It is established that *ptc* is a transcriptional target of Shh signaling, in addition to being a receptor for Shh. Since transcription of *ptc* is upregulated in Shh receiving cells, *ptc* expression can be used as a marker of activation of Shh signaling (Marigo et al., 1996a; Goodrich et al., 1996). To test a possibility that Shh signaling is indeed activated at the anterior mesoderm in the $ptc^{-/mes}$, the expression of *ptc* was analyzed. For this purpose, *lacZ* gene inserted into the *ptc* knockout locus was used to monitor *ptc* expression. Since β-galactosidase is very stable in cells (Enchelard et al., 1994), weak and transient expression was expected to be detected. As shown in Fig. 16, β-gal staining indicated that *ptc* was expressed in the posterior half of both fore- and hindlimbs in 11.5 dpc $ptc^{-/+}$ embryos with gradient from posterior to anterior, as

previously reported (Marigo et al., 1996a). In $ptc^{-/mes}$ embryos, no significant alteration of the expression domain of *ptc* was observed in all eight embryos analyzed. Furthermore, the same result was obtained in 11 and 12 dpc embryos (Fig.16a, c). All results indicated that in the anterior mesenchymal cells Shh signaling was not activated, or only activated under detectable level.

4. Discussion

4. 1 Neonatal lethality of *ptc*$^{-/mes}$ mice and abnormal lung development

This study demonstrated that the compound heterozygotes of *mes* and *ptc* knockout alleles showed neonatal death due to a defect in the respiration. Detailed analysis indicated that the pulmonary alveoli were not formed in the *ptc*$^{-/mes}$ embryos because of overgrowth of the mesenchymal cells. To clarify whether this hyperplasia of the mesenchymal cells is derived from alteration of *shh* expression, I analyzed expression of *shh*. The preliminarily result showed no marked alteration of *shh* expression in the lung of *ptc*$^{-/mes}$ embryos, in comparison with that of *ptc*$^{+/+}$embryos (data not shown). From this observation, I inferred that the hyperplasia of *ptc*$^{-/mes}$ lung mesenchyme may result from activation of Shh signaling pathway in *shh* receiving cells, which is caused by the hypomorphic mutation of *ptc*.

Lung phenotype of *ptc*$^{-/mes}$ is very similar to that observed in *shh* overexpressing transgenic mice in which surfactant protein-C (SP-C) gene promoter/enhancer driving *shh* gene was introduced. In the transgenic mice, *shh* was overexpressed throughout the distal epithelium weakly from 10.5 to 15.5 dpc, and highly thereafter (Bellusci et al., 1997b). SP-C-*shh* transgenic mice die soon after birth because of inability of breathing, and abundance of mesenchymal cells was observed without alteration of the D-V axis formation. This result suggested that hypermorph of Shh signaling affects terminal lung development, especially alveoli formation, and Shh signaling is responsible for positive regulation of lung mesenchyme proliferation. Almost identical phenotype observed in the *ptc*$^{-/mes}$ embryos in this study provided a

direct evidence that *ptc* has an essential role in repressing the overgrowth of the lung mesenchymal cell to afford normal alveoli formation.

In addition to the failure of the lung development, I found that five of twenty $ptc^{-/mes}$ embryos exhibited dot hemorrhage in their skin (Fig. 7d). It was reported that $ptc^{-/-}$ embryos died around 10 dpc because of abnormal development of the heart, and that small fraction of the embryos may die because of abnormal vessel formation. These facts indicate that *ptc* has a role in heart and vessel formation. It is also likely that some $ptc^{-/mes}$ embryos died due to inability to pass through the birth channel because of its large body size (see below).

4. 2 Increased body size in $ptc^{-/mes}$ embryos

It was previously reported that reduction of *ptc* activity increases the body size of mice (Milenkovic et al., 1999). Since body size is mainly determined by the number of cells that animal contains (Conlon and Raff, 1999), *ptc* may negatively regulate cell proliferation or positively regulate cell death. As was shown in the present study, both dorsal and ventral mesenchyme overproliferated in $ptc^{-/mes}$ embryos at 13.5 dpc. It is notable that at least dorsal mesenchymal cells proliferated in a region extremely far from the Shh expressing cells. Because the expression patterns of *shh* and a sclerotomal marker *Pax1* were not affected in the $ptc^{-/mes}$ embryos at 11.5 dpc, it is likely that *ptc* acts as a negative growth regulator in cells that do not receive Shh.

4.3 Function of *ptc* in limb development

In this study, I presented that *shh* and *Fgf4* were ectopically expressed at the anterior margin of the limb buds in $ptc^{-/nes}$ embryos. There was a report that when homozygotes of ptc^{-} were partially rescued by transgenesis of methallothionein gene promotor driving *ptc* gene, preaxial polydactyly with weak ectopic expression of *shh* was observed (Milenkovic et al. 1999). Together with that report, the present result indicated that partial disruption of *ptc* activity give rise to the induction of ectopic expression of *shh* at anterior mesenchyme, suggesting that normal *ptc* acts to repress the *shh* expression at anterior mesenchyme in developing limb buds.

The ectopic expression of *shh* in the limb buds of the $ptc^{-/nes}$ embryos was, however, very weak when compared with that of other mutant mice with preaxial polydactyly, even though the limb phenotype of the $ptc^{-/nes}$ was as severe as those of other mutants. On the other hand, the ectopic expression of *Fgf4* was very strong, being comparable to that of other mutants. These results indicated that the mechanism by which the $ptc^{-/nes}$ mice exhibit the polydactyly is different from that of other mutants. It is well established that if *shh* is applied to anterior mesenchyme, *Fgf4* is ectopically expressed at the anterior ectoderm and duplicated digits are formed. In addition, ectopic expression of *shh* and *Fgf4* was observed in mouse mutants that exhibit preaxial polydactyly, including *Xt*, *Hx*, *Xpl*, *lst* and *Rim4* (Masuya et al., 1995, 1997). These facts infer that anterior mesenchymal cells have potential to respond to Shh, and some factors expressed in anterior mesenchyme repress the ectopic expression of *shh* in normal limb development. It is reported that at least *Gli3* and *Alx4* genes, normally expressed at anterior mesenchyme of limb buds, act to repress the potential expression

of *shh* at anterior mesenchyme (Masuya et al., 1995; Qu et al., 1997). Disruption of either *Gli3* or *Alx4* induces ectopic expression of *shh* and the positive feedback loop between *shh* and *Fgf4* is formed. Strong ectopic expression of *shh* and *Fgf4* is observed in the mice with a mutation in either one of the two genes. Since the function of these negative regulators, *Gli3* and *Alx4*, remains intact in the $ptc^{-/mes}$ embryos, formation of a new positive feedback loop at the anterior mesenchyme may not take place. This may explain why the ectopic expression of *shh* was so weak.

As described above, comparing with the very weak ectopic expression of *shh,* ectopic expression of *Fgf4* in the $ptc^{-/mes}$ embryos was as strong as that of other polydactylous mutants. There are two possibilities to explain this. If in $ptc^{-/mes}$ limb buds Shh signaling is activated to some extent by weakened Ptc activity at the anterior mesenchyme, this subtle activation of Shh pathway might be sufficient for induction of strong ectopic expression of *Fgf4*. This scenario assumes that *Fgf4* induction is highly sensitive to weak activation of Shh signaling. Alternatively, the second interpretation hypothesizes that there is a bifurcation in the Shh signaling pathway. One is the well known pathway to activate expression of *ptc* and *Gli* genes through a transcription factor Gli (Marigo et al., 1996a, b), and the other is that to activate expression of *Fgf4* and *HoxD*, either directly or indirectly. The latter step is independent of Gli transcription factor. *ptc* gene acts to repress the signal transduction in both cascades after the branch point of the bifurcated pathway. This bifurcation pathway is reminiscent of what was observed in chick polydactylous limb mutant talpid^3 (ta^3) (Izpisua-Belmonte et al., 1992; Francis-West et al., 1995). In this mutant, normally

posteriorly restricted *HoxD, Bmp* and *Fgf4* genes are expressed symmetrically across the entire anterposterior axis, but *shh* expression is still restricted to the posterior limb. Moreover, recently it was shown that *ptc* expression is significantly reduced in ta^3 and that function of wild-type ta^3 gene is required for normal response to Shh signals (Lewis et al., 1999). Thus, it is likely that the ta^3 gene product is a component necessary to repress induction of *Fgf4* but not of *ptc* and *Gli* genes, after the branch point of the bifurcated pathway of Shh signaling. In this context, it is notable that in the $ptc^{-/mes}$ limb buds I could not detect the ectopic *ptc* expression at the anterior mesenchyme, which is observed in other preaxial polydatyly mutants.

If this bifurcation pathway is present in mouse limb buds, the C-terminal cytoplasmic domain of Ptc protein, which is disrupted in *mes* mutation, may be involved in the repression of only the cascade that activates *Fgf4* expression. Since the ptc^{mes} product is still able to repress the activation of *ptc* and *Gli* genes, the C-terminal cytoplasmic domain is not necessary for the repression of signal transduction leading to *ptc* and *Gli* genes. Although ta^3 gene is not molecularly identified, it is possible that ta^3 gene products interact to the C-terminal cytoplasmic domain of Ptc protein to repress the transduction of the Shh signal in one of the bifurcated cascades to activate *Fgf4* and *HoxD* genes.

In normal development, expression of *ptc* is not observed at anterior mesoderm by both RNA *in situ* hybridization and X-gal staining. Why does ectopic activation of *shh* signaling occur in the anterior mesoderm of $ptc^{-/mes}$ limb buds? One possible explanation is that *ptc* is expressed in the anterior mesoderm under a detectable level. If

Shh protein or *shh* expressing virus are applied in anterior mesnchyme, *ptc* and *Gli* are ectopically expressed in the surrounding mesenchyme (Marigo et al., 1996a, b). Since *ptc* and *Gli* are target genes of Shh signaling, these anterior cells must have competence to respond to Shh. This implies that in normal condition *ptc* may be expressed at undetectable level at anterior mesenchyme of limb buds.

In addition to the function as a transducer of Shh signaling, it was proposed from the study of wing development of *Drosophilla* (Chen and Stuhl, 1996) that high-level of Ptc protein has the second function to sequester Shh and prevent its diffusion. Therefore, it is possible that in absence or reduction of *ptc* activity, Shh protein is diffusing further and can act over a long distance than normal condition. In this study, I could not investigate the binding affinity of Ptc^{mes} to Shh. If Shh binds to Ptc^{mes} with lower affinity than to wild-type Ptc, Shh molecules may migrate from posterior further to anterior mesenchyme due to incomplete sequestration by high level expression of ptc^{mes} in the posterior mesenchyme. In consequence, the migrated Shh protein may activate Shh signaling pathway at anterior mesenchyme, leading preaxial polydactyly. If the Ptc^{mes} protein has lower binding affinity to Shh molecule, this possibility should be taken in consideration again.

CHAPTER V General discussion

Shh signaling pathway controls many developmental events by inducing specific cell fates or regulating cell proliferation. This pathway controls patterning and growth of limb bud, lung, neural tube and so on. Ptc protein, a receptor for Shh molecule, appears to oppose Shh signaling by repressing activity of Smo molecule that transduce Shh signaling to the downstream genes.

In this study, first I showed that mesenchymal dysplasia (*mes*), a dysmorphological mouse mutation, has a 32-bp deletion of the C-terminal cytoplasmic domain of Ptc protein. Further allelism test of *mes* for *ptc* knockout allele (ptc^-) indicated that *mes* is a hypomorphic allele of the *ptc* gene.

Early embryonic lethality of the ptc^- homozygotes has so far hampered the study of the function of *ptc* in later stages of development. In this study, I analyzed the phenotypes of mice with different combination of *ptc* mutant alleles in order to understand the functions of *ptc* in organogenesis in later developmental stages. Although it was reported that ptc^- homozygous embryos, which die around 10 dpc, exhibit a ventralized and open neural tube (Goodrich et al., 1997), I could not detect these abnormalities in the compound heterozygotes of *mes* and the *ptc* knockout alleles. The $ptc^{-/mes}$ embryos, however, survived till just after birth and exhibited severe phenotypes in many different organs, including overgrowth of the mesenchymal cells, preaxial polydactyly and aplasia of lung alveoli. Less severe phenotype was observed in the same organs of *mes* homozygotes.

One possible interpretation for these different phenotypes depending on the combination of *ptc* alleles is a dose effect of *ptc* activity. If this is the case, different threshold of Shh signaling level required in different organogenesis may explain for the variation of the phenoypes. For example, lung, limb and mesenchyme may be highly sensitive to Shh signaling but neural tube comparably less sensitive.

The second possibility is that the C-terminal cytoplasmic domain of *ptc* plays an important role in development of lung, limb and mesenchyme of trunk, but not in the development of the neural tube. The *ptc*$^{-}$ heterozygotes showed almost no phenotype in limb buds. In contrast, *ptc*$^{-/mes}$ embryos exhibited very severe preaxial polydactyly with strong ectopic *Fgf4* expression at anterior mesenchyme. This fact suggests that the C-terminal cytoplasmic domain of Ptc has an indispensable role in repression of Shh signaling pathway in limb development.

As shown clearly in this study, availability of *mes* mutation has made it possible to study detailed biological roles of *ptc* in later stages of development. Further analysis of the phenotype of especially the compound heterozygotes (*ptc*$^{-/mes}$) would provide a breakthrough in understanding of the *ptc* function in mammalian development.

Some of vertebrate organisms have a secondary member of *ptc* gene, designated as *ptc2*, whose function is still unknown. Ptc2 protein is known to bind Shh proteins, suggesting that *ptc2* may share its role with *ptc* in Shh signaling pathway. It is notable that Ptc2 protein has a short C-teminal cytoplasmic domain like Ptc proteins of fruitfly and fish. From the aspect of evolution, Ptc proteins of only higher vertebrates

such as chick and mammalian have long C-terminal cytoplasmic domain. Considering that the *ptc*$^{-/mes}$ embryos exhibited abnormality in lung development, namely aplasia of pulmonary alveoli, it is of interest to hypothesize that the long C-terminal cytoplasmic domain of Ptc protein was acquired in evolution of warm-blooded animals, being associated with appearance of lung as respiration system.

Acknowledgements

I wish to express my sincere gratitude to my supervisor, Dr. Toshihiko Shiroishi, for his continuous advises, stimulating discussion and encouragement during all the stages of this work.

I am grateful to Drs. Hiromichi Yonekawa, Yasuhiro Hashimoto, Masato Nakafuku and Shinichi Fukami for their collaboration and discussion.

I also thank Drs. Tetsuichiro Saito and Masaru Tamura for giving instructions of *in situ* hybridization and helpful suggestions.

I greatly appreciate Drs. Hiroshi Masuya, Junko Ishijima and Tsuyoshi Koide, and Miss Yukari Yada, and other members of Mammalian Genetics Laboratory for valuable suggestions and supporting for this work. I also thank Mr. Akihiko Mita, Mrs. Katsue Aida and Michiko Arii, and other staffs of animal facility of the National Institute of Genetics for taking care of the mice used in this study.

REFERENCE

Alcedo, J., Ayzenzon, M., Ohlen, T. V., Noll, M., and Hooper, J. E. (1996). The Drosophila *smoothened* gene encodes a seven-pass membrane protein, a putative receptor for the Hedgehog signal. Cell 86, 221-232.

Belloni, E., Muenke, M., Roessler, E., Traverso, G., Siegel-Bartelt, J., Frumkin, A., Mitchell, H. F., Donis-Keller, H., Helms, C., Hing, A. V., Heng, H. H. Q., Koop, B., Martindale, D., Rommens, J. M., Tsui, L.-C., and Scherer, S. W. (1996). Identification of *Sonic hedgehog* as a candidate gene responsible for holoprosencephaly. Nat. Genet. 14, 353-356.

Bellusci, S., Henderson, R., Winnier, G., Oikawa, T., and Hogan, B. L. M. (1996). Evidence from normal expression and targeted misexpression that *Bone Morphogenetic protein-4* (*Bmb-4*) plays a role in mouse embryonic lung morphogenesis. Development 122, 1693-1702.

Bellusci, S., Grindley, J., Emoto, H., Itoh, N., and Hogan, B. L. M. (1997a). Fibroblast growth factor 10 (FGF10) and branching morphogenesis in the embryonic mouse lung. Development 124, 4867-4878.

Bellusci, S., Furuta, Y., Rush, M. G., Henderson, R., Winnier, G., and Hogan, B. L. M.

(1997b). Involvement of Sonic hedgehog (*Shh*) in mouse embryonic lung growth and morphogenesis. Development 124, 53-63.

Birren, S. J., Lo, L., and Anderson, D. J. (1993). Sympathetic neuroblasts undergo a developmental switch in trophic dependence. Development 119, 597-610.

Bitgood, M. J., and McMahon, A. P. (1995). *Hedgehog* and *Bmp* genes are coexpressed at many diverse sites of cell-cell interaction in the mouse embryo. Dev. Biol. 172, 126-138.

Capdevila, J., Estrada, M. P., Sanchez-Herrero, E., and Guerrero, I. (1994). The *Drosophila* segment polarity gene *patched* interacts with *decapentaplegic* in wing development. EMBO J. 13, 71-82.

Carpenter, D., Stone, D. M., Brush, J., Ryan, A., Armanini, M., Frantz, G., Rosenthal, A., and de Sauvage., F. J. (1998). Characterization of two patched receptors for the vertebrate hedgehog protein family. Proc. Natl. Acad. Sci. USA 95, 13630-13634.

Chai, C. K. (1981). Dactylaplasia in mice. A two-locus model for developmental anomalies. J. Hered. 72, 234-237.

Chen, Y., and Stuhl, G. (1996). Dual roles for Patched in sequestering and transducing

Hedgehog. Cell 87, 553-563.

Chiang, C., Litingtung, Y., Lee, E., Young, K. E., Corden, J. L., Westphal, H., and Beachy, P. A. (1996). Cyclopia and defective axial patterning in mice lacking *Sonic hedgehog* gene function. Nature 383, 407-413.

Concordet, J.-P., Lewis, K. E., Moore, J. W., Goodrich, L. V., Johnson, R. L., Scott, M. P., and Ingham, P. W. (1996). Spatial regulation of a zebrafish *patched* homologue reflects the role of *sonic hedgehog* and protein kinase A in neural tube and somite patterning. Development 122, 2835-2846.

Conlon, I., and Raff, M. (1999). Size control in animal development. Cell 96, 235-244.

Deutsch, U., Dressler, G. R., and Gruss, P. (1988). *Pax1*, a member of a paired box homologous murine gene family, is expressed in segmented structures during development. Cell 53, 617-625.

Echelard, Y., Epstein, D. J., St-Jacques, B., Shen, L., Mohler, J., McMahon, J. A., and McMahon, A. P. (1993). Sonic Hedgehog, a member of a family of putative signaling molecules, is implicated in the regulation of CNS polarity. Cell 75, 1417-1430.

Enchelard, Y., Vassileva, G., and McMahon, A. P. (1994). *Cis*-acting regulatory

sequence governing *Wnt-1* expression in the developing mouse CNS. Development 120, 2213-2224.

Ericson, J., Morton, S., Kawakami, A., Roelink, H., and Jessell, T. M. (1996). Two critical periods of Sonic Hedgehog signaling required for the specification of motor neuron identity. Cell 87, 661-673.

Fan C.-H., and Tessier-Lavigne, M. (1994). Patterning of mammalian somites by surface ectoderme and notochord: evidence for sclerotome induction by a Hedgehog homolog. Cell 79, 1175-1186.

Fan, H., Oro, A. E., Scott, M. P., and Khavari, P. A. (1997). Induction of basal cell carcinoma features in transgenic human skin expressing Sonic Hedgehog. Nat. Med. 3, 788-792.

Francis-West, P. H., Robertson, K. E., Ede, D. A., Rodriguez, C., Izpisua-Belmonte, J.-C., Houston, B., Burt, D. W., Gribbin, C., Brickell, P. M., and Tickle, C. (1995) Expression of genes encoding Bone Morphogenetic Proteins and Sonic Hedgehog in Talpid limb buds: their relationships in the signaling cascade involved in limb patterning. Dev. Dyn. 203, 187-197.

Gailani, M. R., Stahle-Backdahl, M., Leffell, D. J., Glynn, M., Zaphiropoulos, P. G.,

Pressman, C., Unden, A. B., Dean, M., Brash, D. E., Bale, A. E., and Toftgard, R. (1996). The role of the human homologue of *Drosophila patched* in sporadic basal cell carcinomas. Nat. Genet. 78-81.

Goodrich, L. V., Johnson, R. L., Milenkovic, L., McMahon, J. A., and Scott, M. P. (1996). Conserrvation of the *hedgehog/patched* signaling pathway from flies to mice: induction of a mouse *patched* gene by Hedgehog. Genes Dev. 10, 301-312.

Goodrich, L. V., Milenkovic, L., Higgins, K. M., and Scott, M. P. (1997). Altered neural cell fates and medulloblastoma in mouse *patched* mutants. Science 277, 1109-1113.

Gorlin, R. J. (1987). Nevoid basal-cell carcinoma syndrome. Medicine 66, 98-113.

Hahn, H., Wicking, C., Zaphiropoulos, P. G., Gailani, M. R., Shanley, S., Chidambaram, A., Vorechovsky, I., Holmberg, E., Unden, A. B., Gillies, S., Negus, K., Smyth, I., Pressman, C., Leffell, D. J., Gerrard, B., Goldstein, A. M., Dean, M., Toftgard, R., Chenevix-Trench, G., Wainwright, B., and Bale, A. E. (1996). Mutations of the human homolog of Drosophila *patched* in the nevoid basal cell carcinoma syndrome. Cell 85, 841-851.

Hahn H., Wojnowski, L., Zimmer, A. M., Hall, J., Miller, G., and Zimmer, A. (1998). Rhabdomyosarcomas and radiation hypersensitivity in a mouse model of Gorlin

syndrome. Nat. Med. 4, 619-622.

Hahn, H., Wojnowski, L., Miller, G., and Zimmer, A. (1999). The patched signaling pathway in tumorigenesis and development: lessons from animal models. J. Mol. Med. 77, 459-468.

Hammerschmidt, M., Brook, A., and McMahorn, A. P. (1997). The world according to *hedgehog*. Trends Genet. 13,14-21.

Hogan, B. L. M. (1999). Morphogenesis. Cell 96, 225-233.

Hooper, J. E., and Scott, M. P. (1989). The Drosophila *patched* gene encodes a putative membrane protein requred for segmental patterning. Cell 59, 751-765.

Hooper, J. E. (1994). Distinct pathways for autocrine and paracrine Wingless signaling in *Drosophila* embryos. Nature 372, 461-464.

Ingham, P. W., Taylor, A. M., and Nakano, Y. (1991). Role of the *Drosophila patched* gene in positional signaling. Nature 353, 184-187.

Izpisua-Belmonte, L.-C., Ede, D. A., Tickle, C., and Duboule, D. (1992) The mis-expression of posterior *Hox-4* genes in *talpid* (ta^3) mutant wings correlates with the

absence of anteroposterior polarity. Development 114, 959-963.

Johnson, R. L., Laufer, E., Riddle, R. D., and Tabin, C. (1994). Ectopic expression of *Sonic hedgehog* alters dorsal-ventral patterning of somites. Cell 79, 1165-1173.

Johnson, R. L., Rothman, A. L., Xie, J., Goodrich, L. V., Bare, J. W., Bonifas, J. M., Quinn, A. G., Myers, R. M., Cox, D. R., Epstein Jr., E. H., and Scott, M. P. (1996). Human homolog of *patched*, a candidate gene for the basal cell nevus syndrome. Science 272, 1668-1671.

Johnson, R. L., and Tabin, C. J. (1997). Molecular models for vertebrate limb development. Cell 90, 979-990.

Kallasy, M., Toftgard, R., Ueda, M., Nakagawa, K., Vorechovsky, I., Yamasaki, H., and Nakazawa, H. (1997). Patched (*ptch*)-associated preferential expression of Smoothened (*smoh*) in human basal cell carcinoma of the skin. Cancer Res. 57, 4731-4735.

Laufer, E., Nelson, C. E., Johnson, R. L., Morgan, B. A., and Tabin, C. (1994). *Sonic hedgehog* and *fgf-4* act through a signaling cascade and feedback loop to integrate growth and patterning of the developing limb bud. Cell 79, 993-1003.

Lee, J. J., Ekker, S. C., von Kessler, D. P., Porter, J. A., Sun, B. I., and Beachy, P. A.

(1994). Autoproteolysis in *hedgehog* protein biogenesis. Science 266, 1528-1537.

Lewis, K. E., Drossopoulou, G., Paton, I. R., Morrice, D. R., Robertson, K. E., Burt, D. W., Ingham, P. W., and Tickle, C. (1999). Expression of *ptc* and *gli* genes in talpid[3] suggests bifurcation in Shh pathway. Development 126, 2397-2407.

Litingtung, Y., Lei, L., Westphal, H., and Chiang, C. (1998). Sonic hedgehog is essential to forgut development. Nat. Genet. 20, 58-61.

Lopez-Martinez, A., Chang, D. T., Chiang, C., Porter, J. A., Ros, M. A., Simandl, B. K., Beachy, P. A., and Fallon, J. F. (1995). Limb-patterning activity and restricted posterior localization of the amino-terminal product of Sonic hedgehog cleavage. Curr. Biol. 5, 791-796.

Marigo, V., Scott, M. P., Johnson, R. L., Goodrich, L. V., and Tabin, C. J. (1996a). Conservation in *hedgehog* signaling: induction of a chicken *patched* homolog by *Sonic hedgehog* in the developing limb. Development 122, 1225-1233.

Marigo, V., Johnson, R. L., Vortkamp, A., and Tabin, C. J. (1996b). Sonic hedgehog differentially regulates expression of *GLI* and *GLI3* during limb development. Dev. Biol. 180, 273-283.

Masuya, H., Sagai, T., Wakana, S., Moriwaki, K., and Shiroishi, T. (1995). A duplicated zone of polarizing activity in polydactylous mouse mutants. Genes Dev. 9, 1645-1653.

Masuya, H., Sagai, T., Moriwaki, K., and Shiroishi, T. (1997). Multigenic control of the localization of the zone of polarizing activity in limb morphogenesis in the mouse. Dev. Biol. 182, 42-51.

Milenkovic, L., Goodrich, L. V., Higgins, K. M., and Scott, M. P. (1999). Mouse *patched1* controls body size determination and limb patterning. Development 126, 4431-4440.

Motoyama, J., Takabatake, T., Takeshima, K., and Hui, C.-C. (1998). *Ptch2*, a second mouse Patched gene is co-expressed with Sonic hedgehog. Nat. Genet. 18, 104-106.

Nakano, Y., Guerrero, I., Hidalgo, A., Taylor, A., Whittle, J. R. S., and Ingham, P. W. (1989). A protein with several possible membrane-spanning domains encoded by the *Drosophila* segment polarity gene *patched*. Nature 341, 508-513.

Niswander, L., Jeffrey, S., Martin, G. R., and Tickle, C. (1994). A positive feedback loop coordinates growth and patterning in the vertebrate limb. Nature 371, 609-612.

Ohuchi, H., Nakagawa, T., Yamamoto, A., Araga, A., Ohata, T., Ishimaru, Y., Yoshioka,

H., Kuwana, T., Nohno, T., Yamasaki, M., Itoh, N., and Noji, S. (1997). The mesenchymal factor, FGF10, initiates and maintains the outgrowth of the chick limb bud through interation with FGF8, an apical ectodermal factor. Development 124, 2235-2244.

Oro, A. E., Higgins, K. M., Hu, Z., Bonifas, J. M., Epstein Jr., E. H., and Scott, M. P. (1997). Basal cell carcinomas in mice overexpressing Sonic Hedgehog. Science 276, 817-821.

Park W. Y., Miranda, B., Lebeche, D., Hashimoto, G., and Cardoso, W. V. (1998). Fgf-10 is a chemotactic factor for distal epithelial buds during lung development. Dev. Biol. 201, 125-134.

Porter, J. A., von Kessler, D. P., Ekker, S. C., Young, K. E., Lee, J. J., Moses, K., and Beachy, P. A. (1995). The product of *hedgehog* autoproteolytic cleavage active in local and long-range signaling. Nature 374, 363-366.

Porter, J. A., Ekker, S. C., Park, W.-J., von Kessler, D. P., Young, K. E., Chen, C.-H., Ma, Y., Woods, A. S., Cotter, R. J., Koonin, E. V., and Beachy, P. A. (1996a). Hedgehog patterning activity: Role of a lipophilic modification mediated by the carboxy-terminal autoprocessing domain. Cell 86, 21-34.

Porter, J. A., Young, K. E., and Beachy, P. A. (1996b). Cholesterol modification of Hedgehog signaling proteins in animal development. Science 274, 255-259.

Prince, V., and Lumsden, A. (1994). *Hoxa-2* expression in normal and transposed rhombomeres: independent regulation in the neural tube and neural crest. Development 120, 911-923.

Qu, S., Niswender, K. D., Ji, Q., van der Meer, R., Keeney, D., Magnuson, M. A., and Wisdom, R. (1997). Polydactyly and ectopic ZPA formation in *Alx-4* mutant mice. Development 124, 3999-4008.

Riddle, R. D., Johnson, R. L., Laufer, E., and Tabin, C. (1993). *Sonic hedgehog* mediates the polarizing activity of the ZPA. Cell 75, 1401-1416.

Roelink, H., Augsburger, A., Heemskerk, J., Korzh, V., Norlin, S., Ruiz i Altaba, A., Tanabe, Y., Placzec, M., Edlund, T., Jessell, T. M., and Dodd, J. (1994). Floor plate and motor neuron induction by *vhh-1*, a vertebrate homolog of *hedgehog* expressed by the notochord. Cell 76, 761-775.

Roessler, E., Belloni, E., Gaudenz, K., Jay, P., Berta, P., Scherer, S. W., Tsui, L.-C., and Muenke, M. (1996). Mutation in the human *Sonic Hedgehog* gene cause holoprosencephaly. Nature genet. 14, 357-360.

Sambrook, J., Fritsch, E. F., and Maniatis, T. (1989). "Molecular Cloning: A Laboratory Manual," 2nd ed., Cold Spring Harbor Laboratory Press, Cold Spring Harbor, NY.

Schneider, C., King, R. M., and Philipson, L. (1988). Genes specifically expressed at growth arrest of mammalian cells. Cell 54, 787-793.

Sekine, K., Ohuchi, H., Fujiwara, M., Yamasaki, M., Yoshizawa, T., Sato, T., Yagishita, N., Matsui, D., Koga, Y., Itoh, N., and Kato, S. (1999). Fgf10 is essential for limb and lung formation. Nat. Genet. 21, 138-141.

Stone, D. M., Hynes, M., Armanini, M., Swanson, T. A., Gu, Q., Johnson, R. L., Scott, M. P., Pennica, D., Goddard, A., Phillips, H., Noll, M., Hooper, J. E., de Sauvage, F., and Rosenthal, A. (1996). The tumour-supressor gene *patched* encodes a candidate receptor for Sonic hedgehog. Nature 384, 129-134.

Sweet, H. O., Bronson, R. T., Donahue, L. R., and Davisson, M.T. (1996). Mesenchymal dysplasia: A recessive mutation on chromosome 13 of the mouse. J. Hered. 87, 87-95.

Tabata, T., and Kornberg, T. B. (1994). Hedgehog is a signaling protein with a key role in patterning Drosophila imaginal discs. Cell 76, 89-102.

van den Heuvel, M., and Ingham, P. W. (1996). *smoothened* encodes a receptor-like serpentine protein required for *hedgehog* signaling. Nature 382, 547-551.

Weaver, M., Yingling, J. M., Dunn, N. R., Bellusci, S., and Hogan, B. L. M. (1999). Bmp signaling regulates proximal-distal differentiation of endoderm in mouse lung development. development 126, 4005-4015.

Xie, J., Murone, M., Luoh, S.-M., Ryan, A., Gu, Q., Zhang, C., Bonifas, J. M., Lam, C.-W., Hynes, M., Goddard, A., Rosenthal, A., Epstein Jr, E. H., and de Sauvage, F. J. (1998). Activating *Smoothened* mutaions in sporadic basal-cell carcinoma. Nature 391, 90-92.

Zuniga, A., Haramis, A.-P. G., McMahon, A. P., and Zeller, R. (1999). Signal relay by BMB antagonism controls the SHH/FGF4 feedback loop in vertebrate limb buds. Nature 401, 598-602.

Fig. 1 (a)

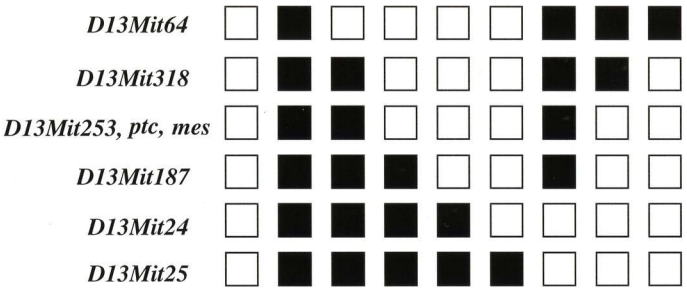

(MSM x B6C3Fe-a/a-*mes*/*mes*)F1 x B6C3Fe-a/a-*mes*/*mes*

N=241

(b)

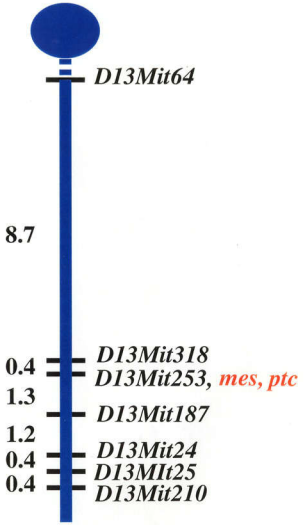

Fig. 1 Gene mapping of *mes* based on the polydactylous phenotype. (MSM x B6C3Fe-a/a-*mes*/*mes*)F1 mice were backcrossed to B6C3Fe-a/a-*mes*/*mes* mice. Using 241 backcross progeny (BCN2), *mes* was mapped to a region between *D13Mit318* and *D13Mit187*. This region included *patched* (*ptc*), and *mes* was not genetically segregated from *ptc*. (a) Haplotype analysis of *mes*. Microsatellite marker loci examined are listed to the left side of the haplotype panel. The number of animals with each haplotype is listed at the bottom of each column. The open squares represent *mes* allele, and the solid squares MSM allele. (b) Genetic map around *mes* in chromosome 13. Microsatellite marker loci examined are shown at the right side of the map. The map distances (in cM) were shown at the left side of the map.

Fig. 2

(a)

3551

CTGAGCCGCCTCCAAGTGTCGTCCGGTTTGCCGTGCCTCC

TGGTCACACGAACAATGGGTCTGATTCCTCCGACTCGGAG

TACAGCTCTCAGACCACGGTGTCTGGCATCAGTGAGGAGC

32 bp deletion

TCAGGCAATACGAAGCACAGCAGGGTGCCGGAGGCCCTGC

3750

CCACCAAGTGATTGTGGAAGCCACAGAAAACCCTGTCTTT

(b)

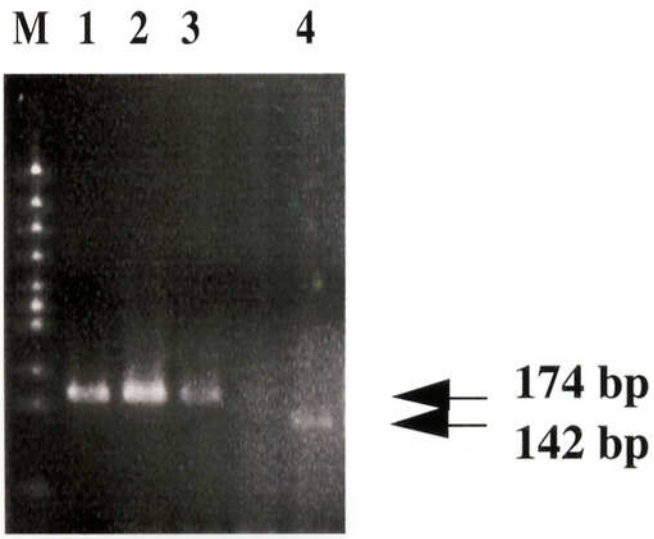

Fig. 2 *mes* has a 32bp-deletion in the C-terminal cytoplasmic domain of *ptc*. (a) Nucleotide sequence of the deletion region of *ptc* in *mes*. *ptc* cDNA obtained from a embryo of *mes* homozygote was sequenced and a 32 bp-deletion was identified. Two arrows indicate primer pair to detect this deletion. (b) PCR products of genomic DNAs from different inbred strains and *mes* mutant, amplified by the same primer pairs used in (a). As *mes* arose in CBA/J strain and has been maintained on B6C3F1 background, PCR product from the genomic DNA of *mes* mutant was expected to have the size identical to either one of three strains, C57BL/6J (lane 1), C3H/HeJ (lane 2) and CBA/J (lane 3). The amplified PCR-product from *mes* mutant (lane 4) showed a unique size (142 bp) shorter than that from above three mouse strains. The length of the nucleotide sequence of *mes ptc* gene was consistent with the size expected from the deletion.

Fig. 3

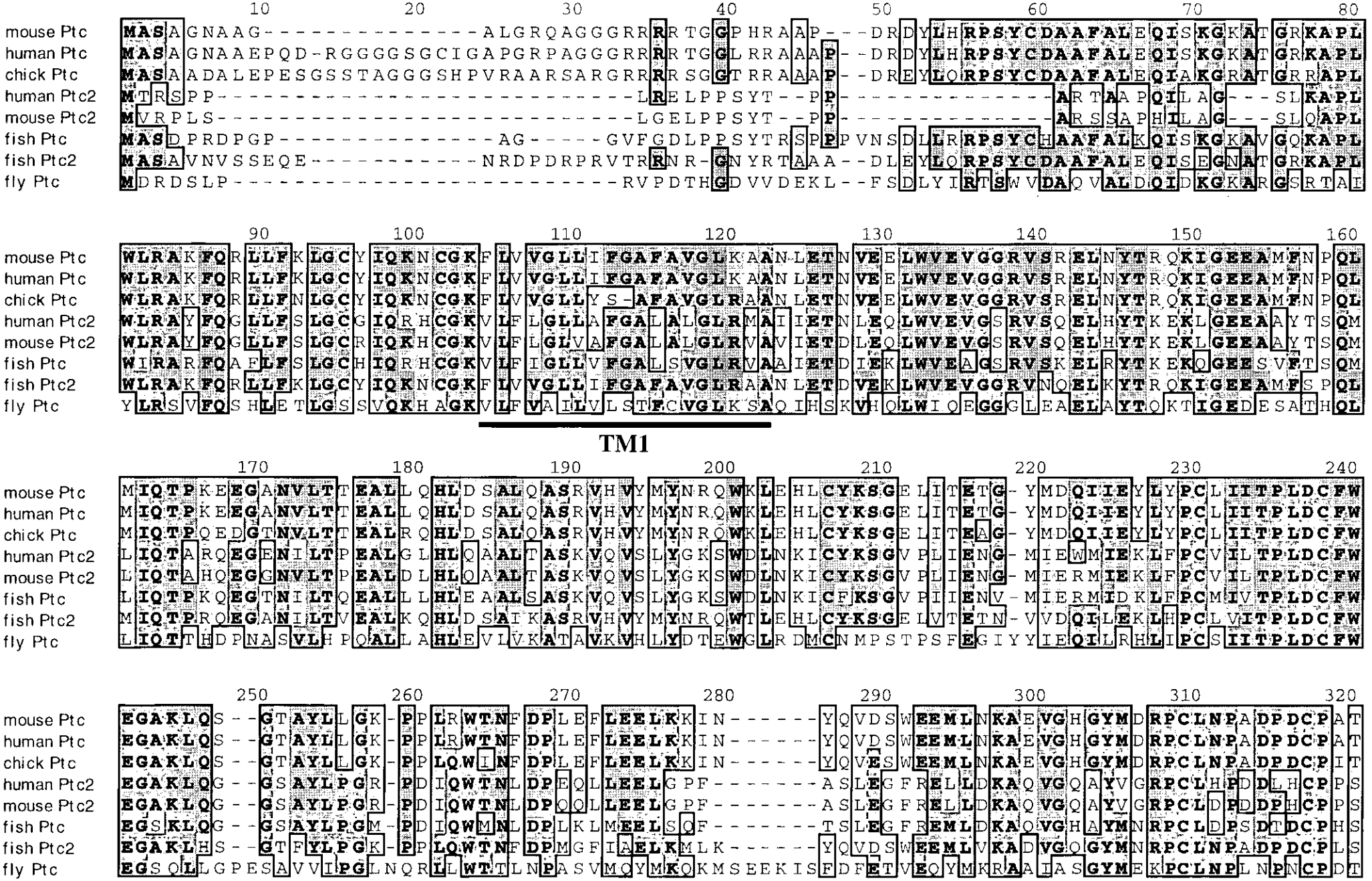
mouse Ptc
human Ptc
chick Ptc
human Ptc2
mouse Ptc2
fish Ptc
fish Ptc2
fly Ptc
TM1

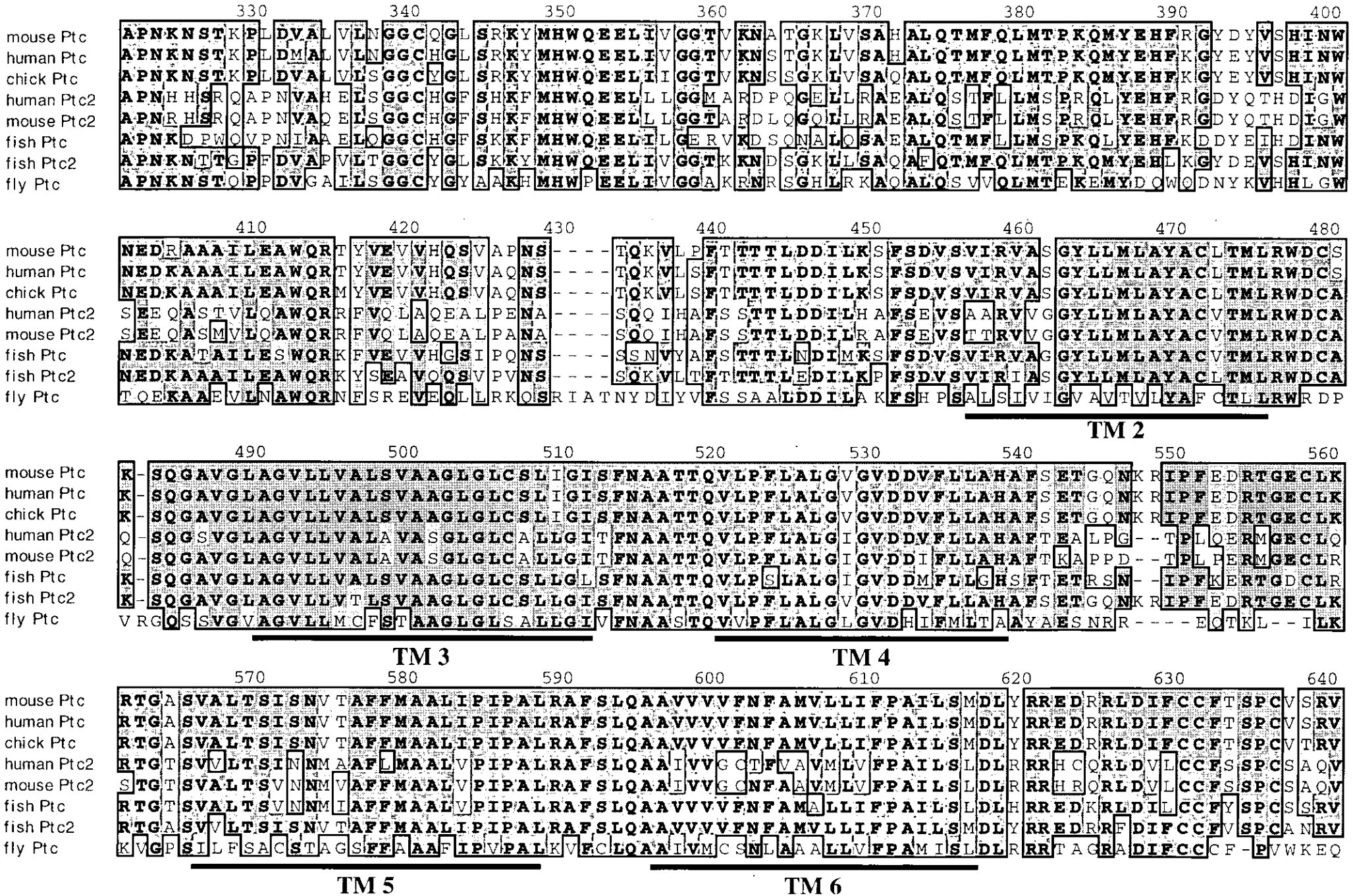
330 340 350 360 370 380 390 400
mouse Ptc
human Ptc
chick Ptc
human Ptc2
mouse Ptc2
fish Ptc
fish Ptc2
fly Ptc
410 420 430 440 450 460 470 480
TM 2
490 500 510 520 530 540 550 560
TM 3
TM 4
570 580 590 600 610 620 630 640
TM 5
TM 6

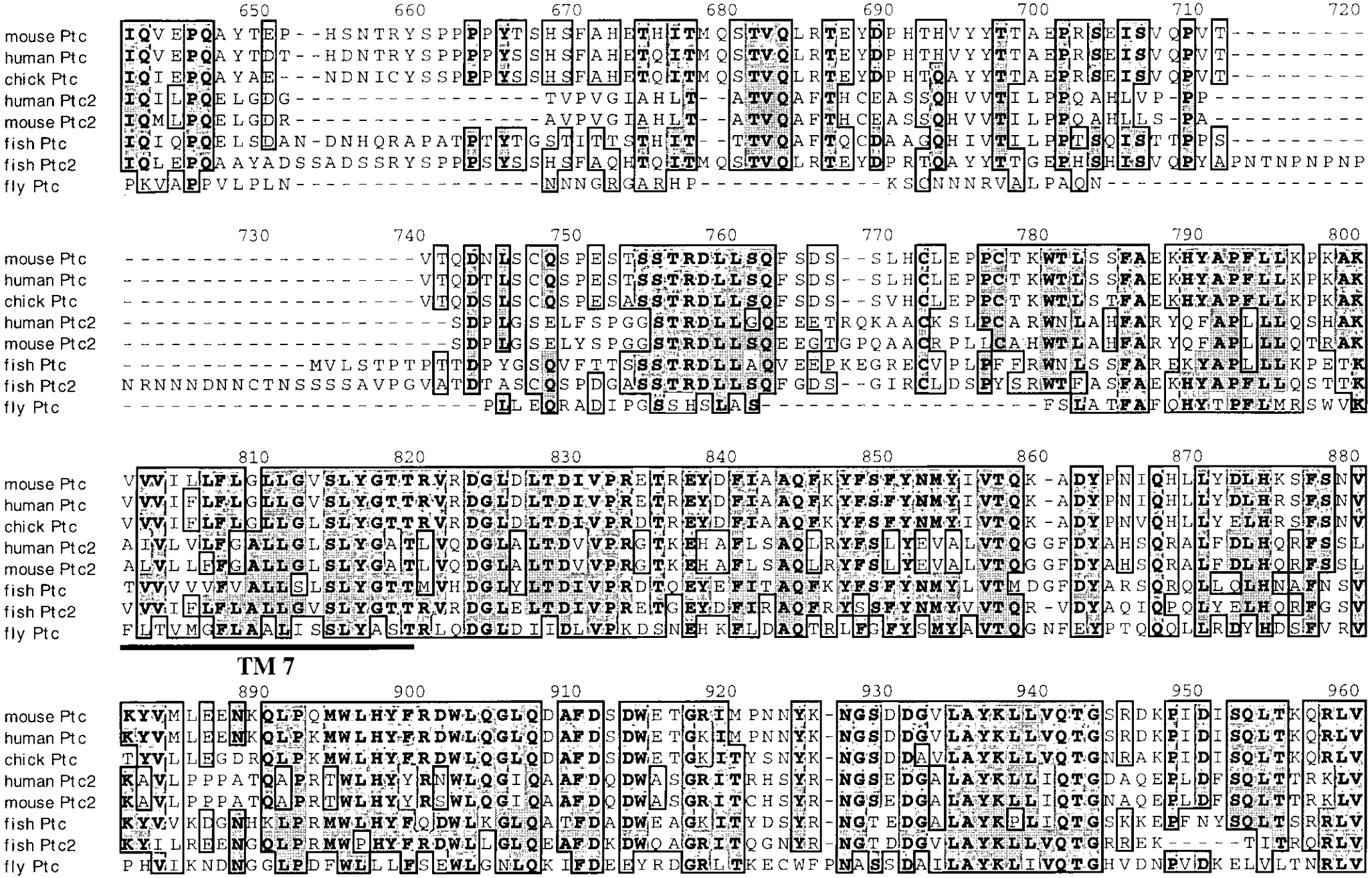
650 660 670 680 690 700 710 720
mouse Ptc
human Ptc
chick Ptc
human Ptc2
mouse Ptc2
fish Ptc
fish Ptc2
fly Ptc
730 740 750 760 770 780 790 800
mouse Ptc
human Ptc
chick Ptc
human Ptc2
mouse Ptc2
fish Ptc
fish Ptc2
fly Ptc
810 820 830 840 850 860 870 880
mouse Ptc
human Ptc
chick Ptc
human Ptc2
mouse Ptc2
fish Ptc
fish Ptc2
fly Ptc
TM 7
890 900 910 920 930 940 950 960
mouse Ptc
human Ptc
chick Ptc
human Ptc2
mouse Ptc2
fish Ptc
fish Ptc2
fly Ptc

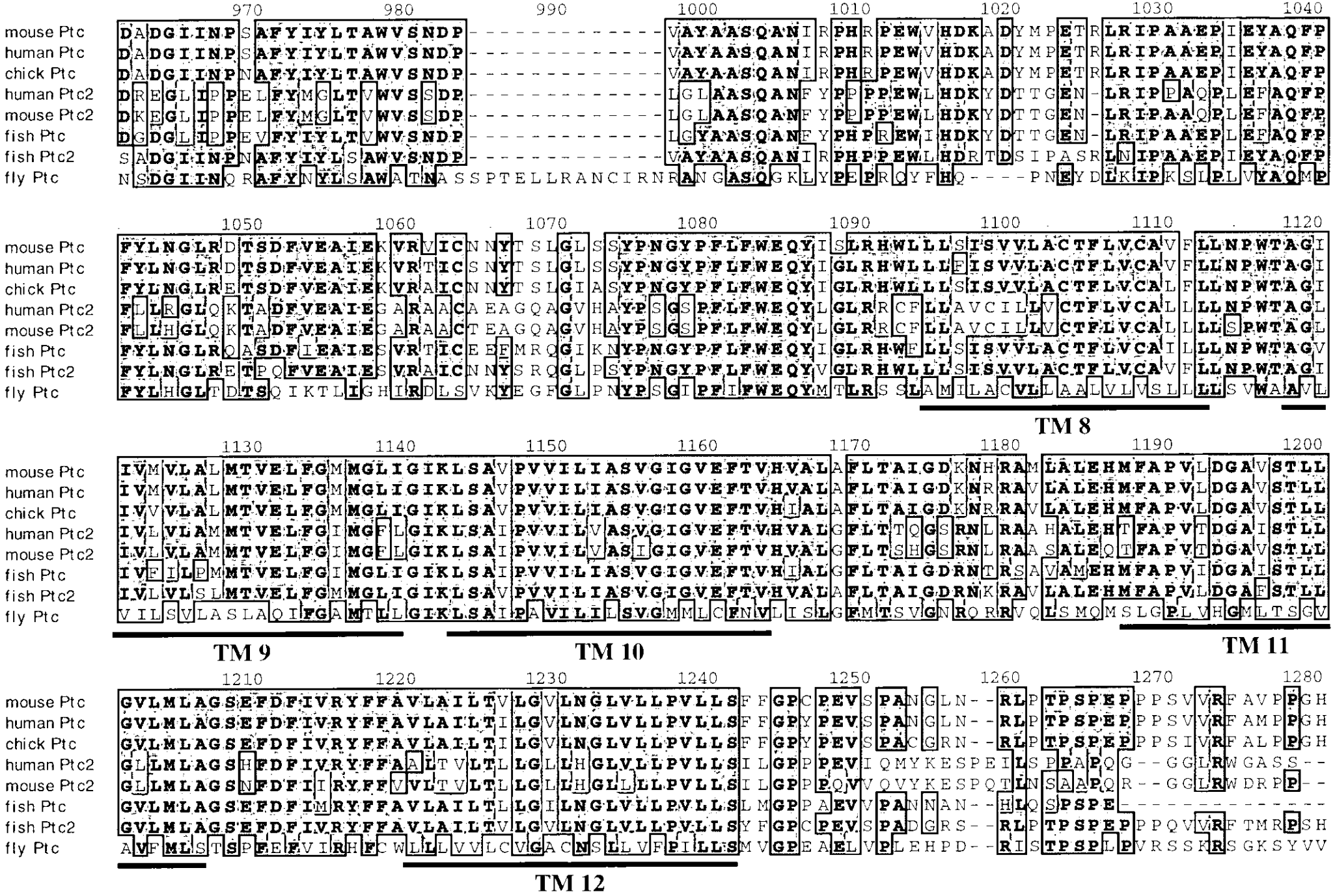
970 980 990 1000 1010 1020 1030 1040
mouse Ptc
human Ptc
chick Ptc
human Ptc2
mouse Ptc2
fish Ptc
fish Ptc2
fly Ptc
1050 1060 1070 1080 1090 1100 1110 1120
TM 8
1130 1140 1150 1160 1170 1180 1190 1200
TM 9
TM 10
TM 11
1210 1220 1230 1240 1250 1260 1270 1280
TM 12

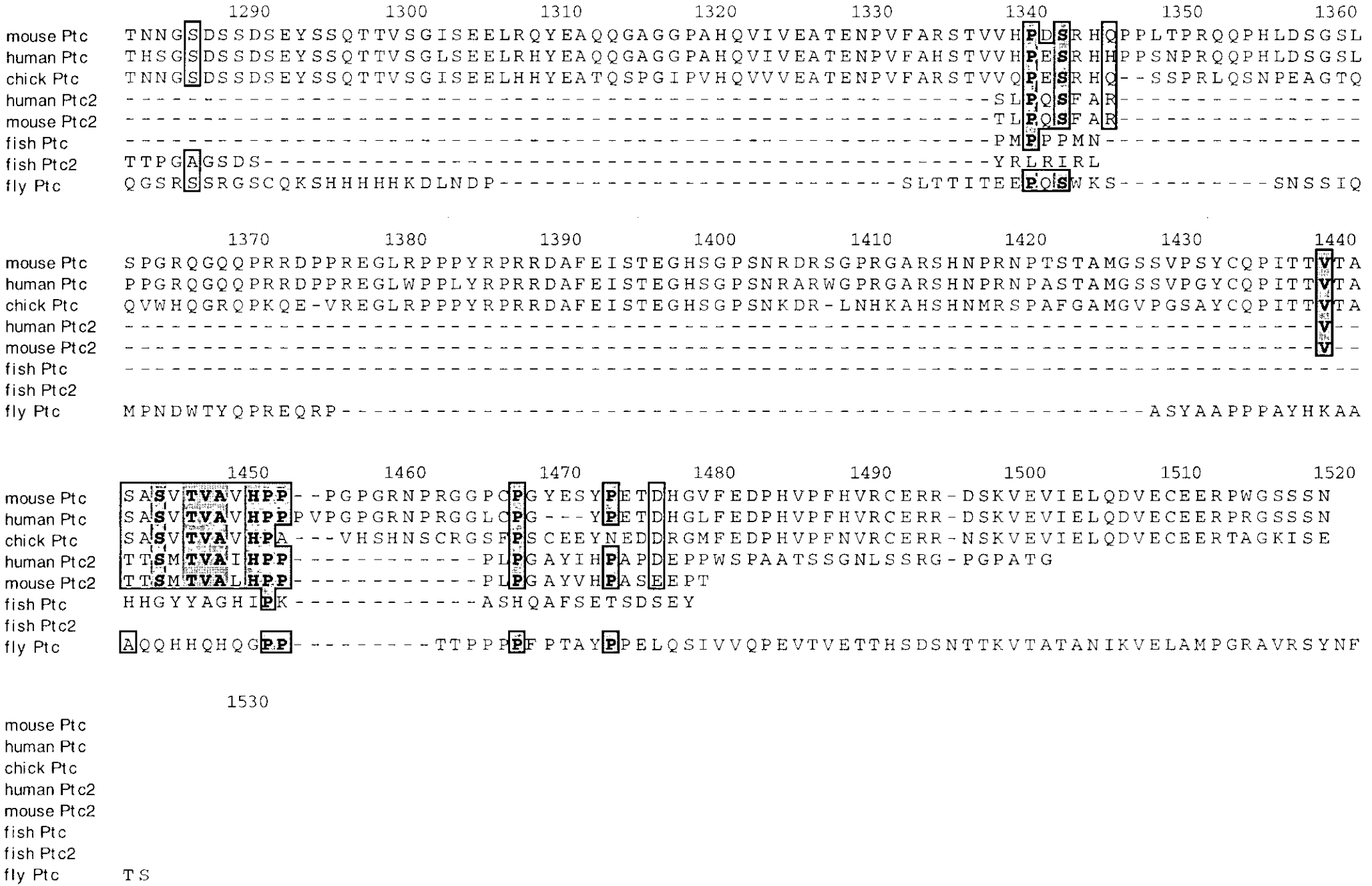
1290 1300 1310 1320 1330 1340 1350 1360
mouse Ptc TNNGSDSSDSEYSSQTTVSGISEELRQYEAQQGAGGPAHQVIVEATENPVFARSTVVHPDSRHQPPLTPRQQPHLDSGSL
human Ptc THSGSDSSDSEYSSQTTVSGLSEELRHYEAQQGAGGPAHQVIVEATENPVFAHSTVVHPESRHHPPSNPRQQPHLDSGSL
chick Ptc TNNGSDSSDSEYSSQTTVSGISEELHHYEATQSPGIPVHQVVVEATENPVFARSTVVQPESRHQ--SSPRLQSNPEAGTQ
human Ptc2 ----------SLPQSFAR----------
mouse Ptc2 ----------TLPQSFAR----------
fish Ptc ----------PMPPPMN----------
fish Ptc2 TTPGAGSDS----------YRLRIRL
fly Ptc QGSRSSRGSCQKSHHHHHKDLNDP----------SLTTITEEPQSWKS----------SNSSIQ
1370 1380 1390 1400 1410 1420 1430 1440
mouse Ptc SPGRQGQQPRRDPPREGLRPPPYRPRRDAFEISTEGHSGPSNRDRSGPRGARSHNPRNPTSTAMGSSVPSYCQPITTVTA
human Ptc PPGRQGQQPRRDPPREGLWPPLYRPRRDAFEISTEGHSGPSNRARWGPRGARSHNPRNPASTAMGSSVPGYCQPITTVTA
chick Ptc QVWHQGRQPKQE-VREGLRPPPYRPRRDAFEISTEGHSGPSNKDR-LNHKAHSHNMRSPAFGAMGVPGSAYCQPITTVTA
human Ptc2 ----------V--
mouse Ptc2 ----------V--
fish Ptc ----------
fish Ptc2
fly Ptc MPNDWTYQPREQRP----------ASYAAPPPAYHKAA
1450 1460 1470 1480 1490 1500 1510 1520
mouse Ptc SASVTVAVHPP--PGPGRNPRGGPCPGYESYPETDHGVFEDPHVPFHVRCERR-DSKVEVIELQDVECEERPWGSSSN
human Ptc SASVTVAVHPPPVPGPGRNPRGGLCPG---YPETDHGLFEDPHVPFHVRCERR-DSKVEVIELQDVECEERPRGSSSN
chick Ptc SASVTVAVHPA---VHSHNSCRGSFPSCEEYNEDDRGMFEDPHVPFNVRCERR-NSKVEVIELQDVECEERTAGKISE
human Ptc2 TTSMTVAIHPP----------PLPGAYIHPAPDEPPWSPAATSSGNLSSRG-PGPATG
mouse Ptc2 TTSMTVALHPP----------PLPGAYVHPASEEPT
fish Ptc HHGYYAGHIPK----------ASHQAFSETSDSEY
fish Ptc2
fly Ptc AQQHHQHQGPP---------TTPPPPFPTAYPPELQSIVVQPEVTVETTHSDSNTTKVTATANIKVELAMPGRAVRSYNF
1530
mouse Ptc
human Ptc
chick Ptc
human Ptc2
mouse Ptc2
fish Ptc
fish Ptc2
fly Ptc TS

Fig. 3 Alignment of amino acids of Ptc and Ptc2 proteins of various species. Dark boxes represent identical amino acid residues, and light boxes represent residues with biochemically similar property. Putative transmembrane domains are underlined.

Fig. 4

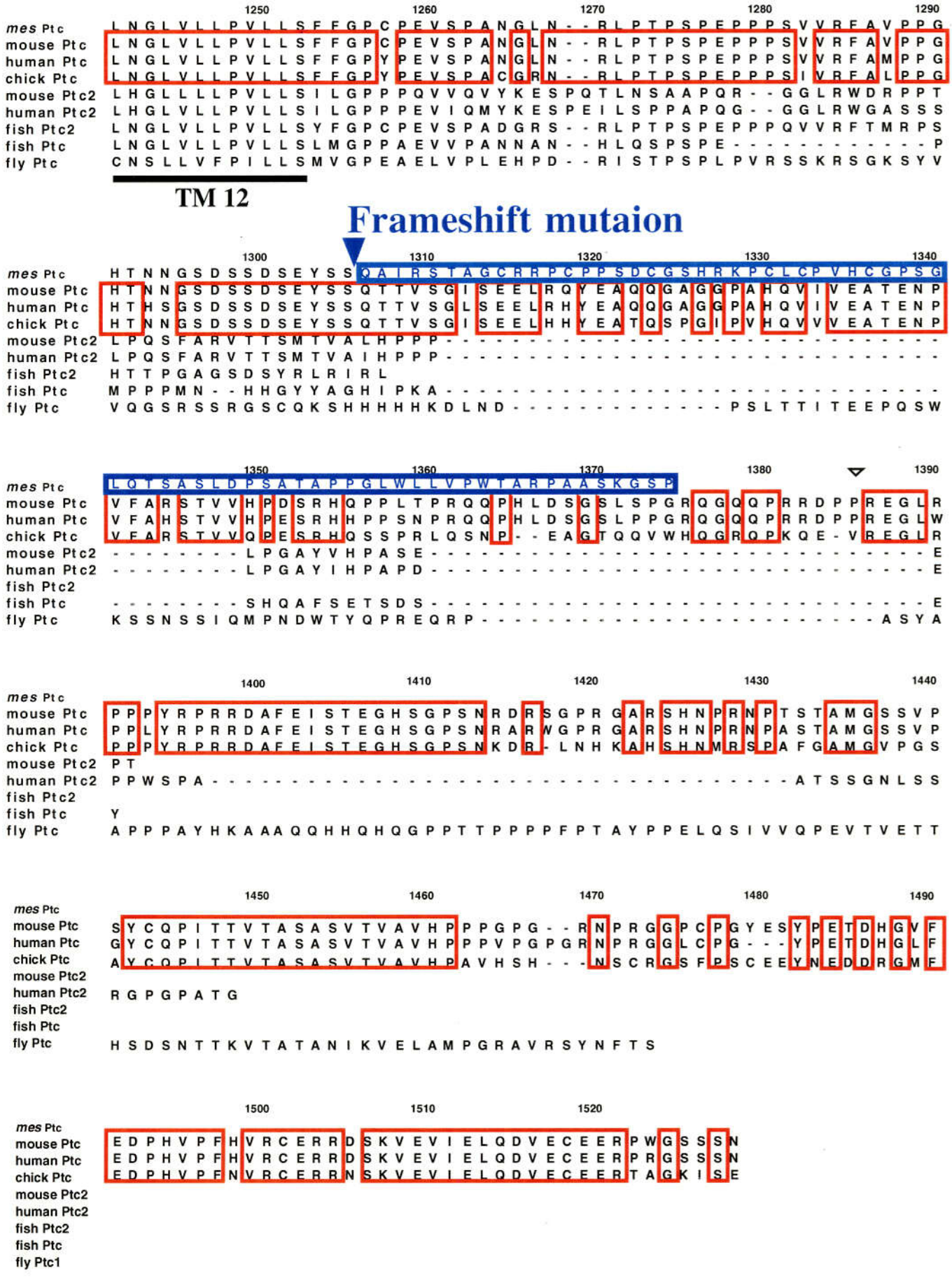
TM 12
Frameshift mutaion
mes Ptc
mouse Ptc
human Ptc
chick Ptc
mouse Ptc2
human Ptc2
fish Ptc2
fish Ptc
fly Ptc
fly Ptc1

Fig. 4 Comparison of amino acid sequences of Ptc and Ptc2 proteins from various species. Only amino acids after transmambrane domain 12 are aligned. Red boxes indicate identical residues among chick, mouse and human Ptc protein. Blue boxes indicate aberrant amino acids following the frameshift mutation in *mes*.

Fig. 5

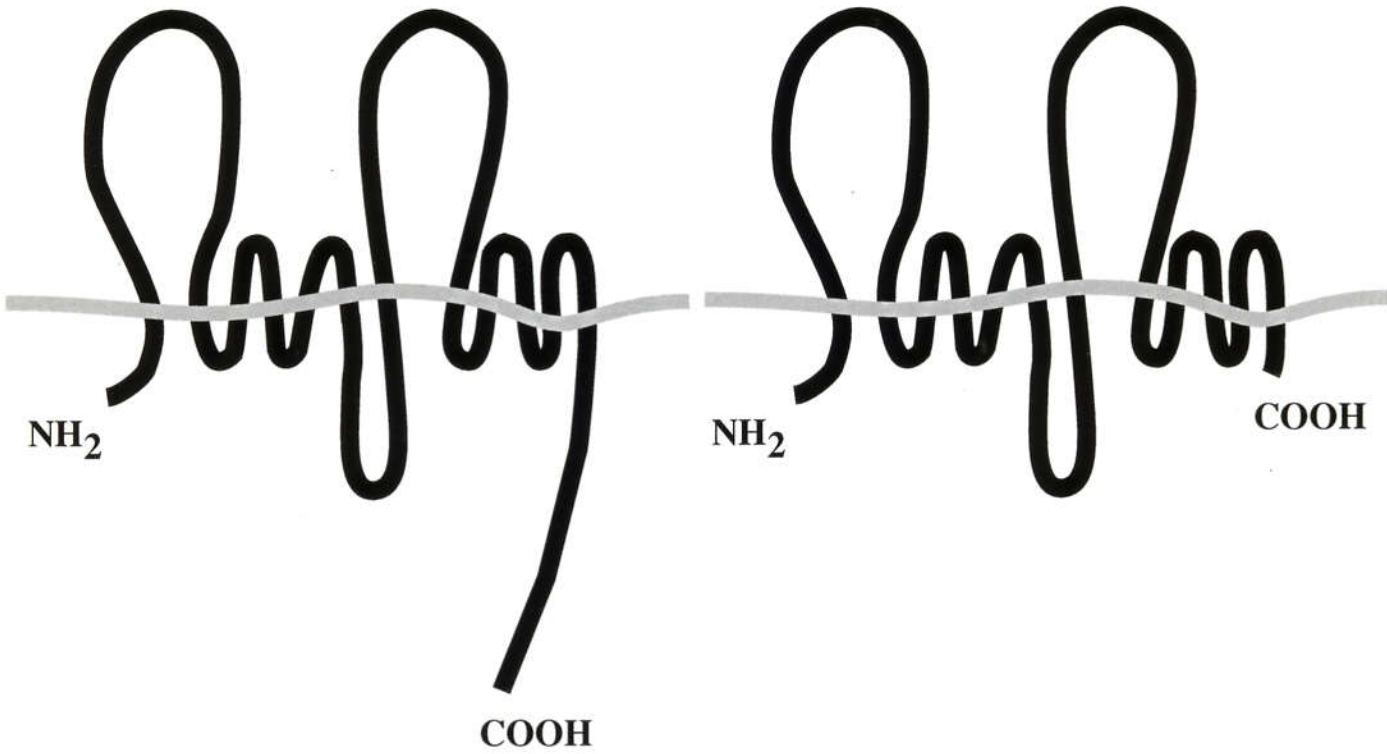

human, chick, mouse Ptc

fly, fish Ptc
fish, mouse, human Ptc2
mes Ptc

Fig. 5 Putative topological models of two types of Ptc. Ptc is highly conserved from fruitfly to human, but there are two divergent regions. One is hydrophilic region between TM6 and TM7. The other is the last C-terminal cytoplasmic domain. This domain of chick, mouse and human Ptc is long and highly conserved, whereas those of fruitfly and fish Ptc, and Ptc2 are short and comparatively divergent. *mes* Ptc can be classified to "short-type" Ptc.

Fig. 6

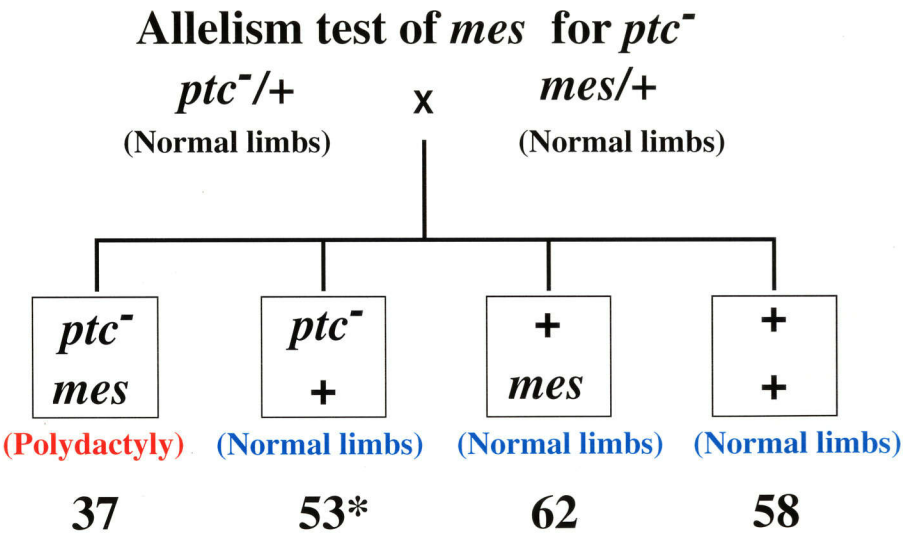
Allelism test of *mes* for *ptc*⁻
ptc⁻/+
(Normal limbs)
x
mes/+
(Normal limbs)
ptc⁻ *mes*
(Polydactyly)
37
ptc⁻ +
(Normal limbs)
53*
+ *mes*
(Normal limbs)
62
+ +
(Normal limbs)
58

Fig. 6 Allelism test of *mes* for *ptc*. Phenotype of the limbs of the embryos generated from the test cross was analyzed from 15.5 dpc to P0 (at birth). Genotype for *mes* allele was determined by PCR using primer pairs capable to detect the 32-bp deletion of *mes*. Genotype for *ptc* knockout allele (*ptc*$^-$) was analyzed by presence or absence of the neomycin resistance gene that was used in targeting vector construction. One of 53 *ptc* single heterozygotes (asterisk) exhibited preaxial polydactyly in only one foot, but this phenotype was much milder than that of compound heterozygotes of both *ptc*$^-$ and *mes* alleles. Each single heterozygotes and wild-type embryos rarely exhibited polydactyly, whereas all embryos with both *ptc*$^-$ and *mes* alleles showed severe preaxial polydactyly. The result indicated that *mes* is an allele at *ptc* locus.

Table 1

Neonatal lethality of *ptc* $^{-/mes}$ embryos from the cross of (*ptc* $^{-/+}$ x *ptc* $^{+/mes}$)

Stage	Genotype of progeny				
	ptc $^{-/mes}$	*ptc* $^{-/+}$	*ptc* $^{+/mes}$	*ptc* $^{+/+}$	Total
11.5 dpc	20 (29%)	13 (19%)	14 (20%)	22 (32%)	69
15.5 dpc	4 (24%)	5 (17%)	9 (31%)	8 (28%)	26
18.5 dpc	18+2* (18%)	29 (26%)	33 (30%)	28 (26%)	110
at birth	1+2* (8%)	10 (27%)	11 (30%)	13 (35%)	37
after 1 week	0 (0%)	22 (33%)	21 (32%)	23 (35%)	66

* Embryos and mice were dead.

Fig. 7

(a)

+/*mes* 13.5 dpc

(c)

-/*mes* 13.5 dpc

(b)

-/*mes* 13.5 dpc

(d)

-/*mes* 18.5 dpc

Fig. 7 Comparison of phenotypes of $ptc^{-/mes}$ embryos and the control littermates. Lateral view of 13.5 dpc embryos of $ptc^{+/mes}$ (a) or $ptc^{-/mes}$ (b, c). $ptc^{-/mes}$ embryo exhibited increased body size, especially in dorsal mesenchyme. At 18.5 dpc, $ptc^{-/mes}$ embryos were 38% heavier than their $ptc^{+/+}$ littermates. Five of 20 embryos (25%) exhibited dot hemorrhage in their skin (d), possibly caused by abnormal vessel formation.

Fig. 8

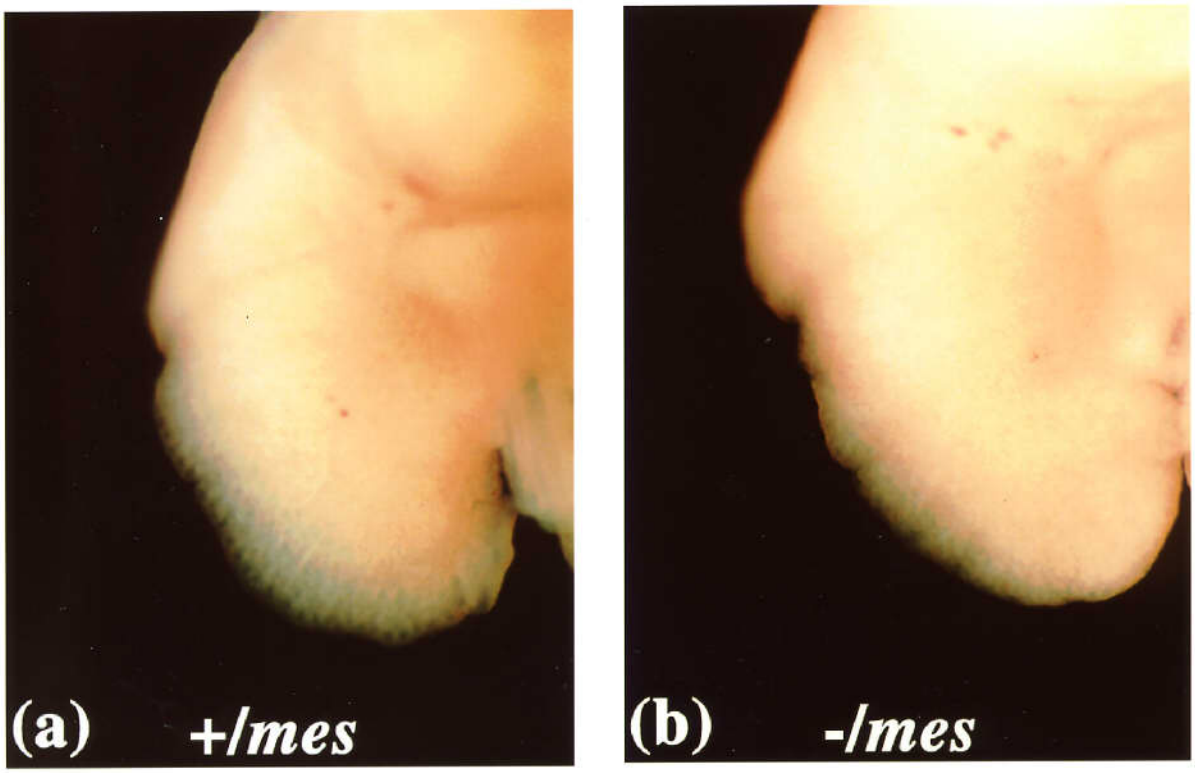

16.5 dpc

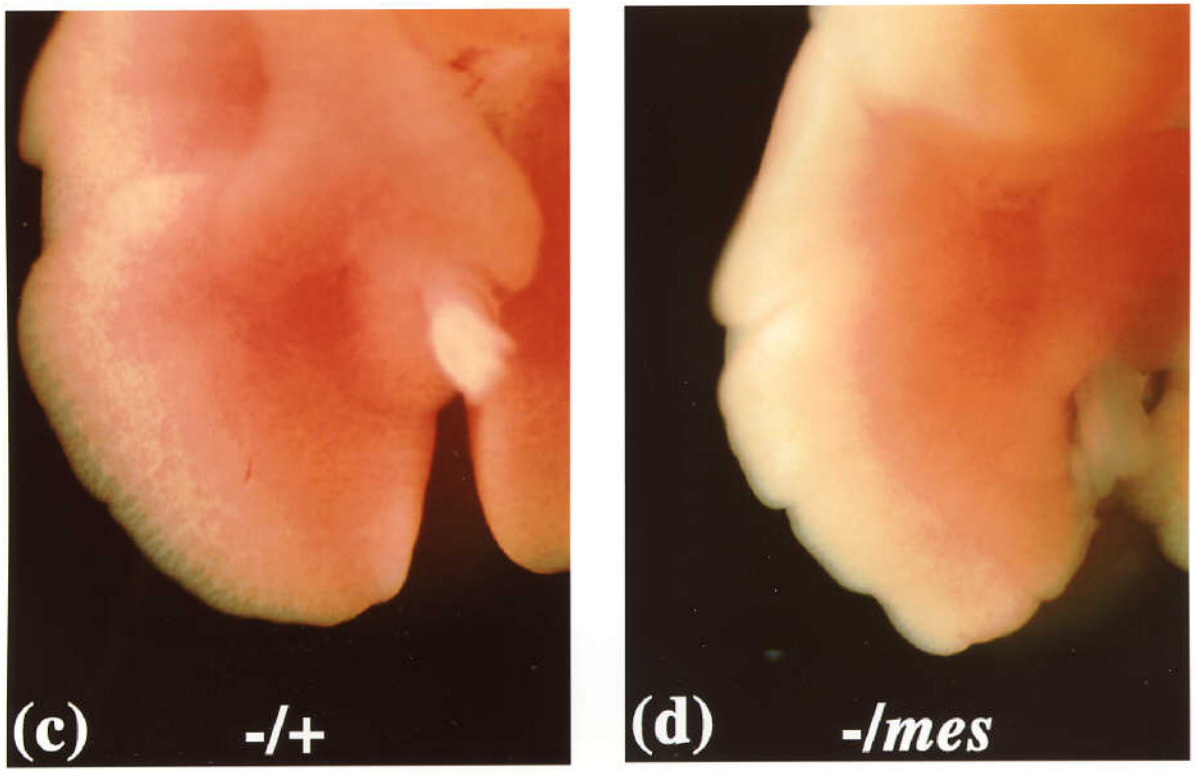

18.5 dpc

Fig. 8 Macroscopic analysis of lungs of $ptc^{-/nes}$ embryo. At 16.5 dpc, no visible difference was observed between $ptc^{+/nes}$ (a) and $ptc^{-/nes}$ (b) lungs. At 18.5 dpc, lung of $ptc^{-/nes}$ (d) was smaller than that of $ptc^{-/+}$ littermates (c), and bronchioles were not observed in $ptc^{-/nes}$ lung.

Fig. 9

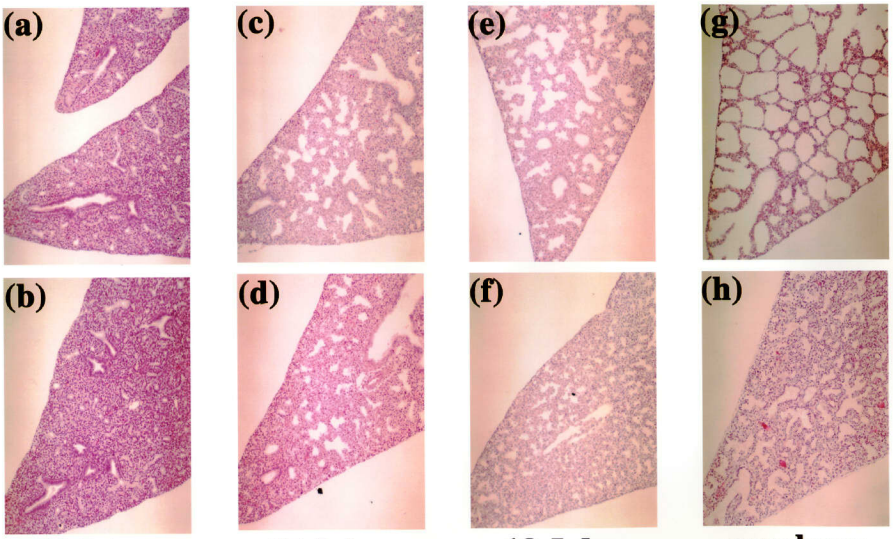

Fig. 9 Abnormal lung development of *ptc*$^{-/nes}$ embryos and new born mice. Section of 16.5 dpc *ptc*$^{-/nes}$ lung (b) showed no significant difference from that of *ptc*$^{+/+}$ embryo (a). At 17.5 dpc, the mesenchyme of *ptc*$^{-/nes}$ lung (d) likely overgrew than that of *ptc*$^{+/+}$ embryo (c). Subsequently, at 18.5 dpc, the airway of *ptc*$^{-/nes}$ lung (f) was thinner than that of *ptc*$^{+/+}$ embryo (e), and the mesenchyme of *ptc*$^{-/nes}$ lung further overgrew. In new born mice, many alveoli were formed in lung of *ptc*$^{+/+}$ mice (g), while not in *ptc*$^{-/nes}$ (h). This suggests that *ptc* has a function of negative regulation in cell growth of lung mesenchyme.

Fig. 10

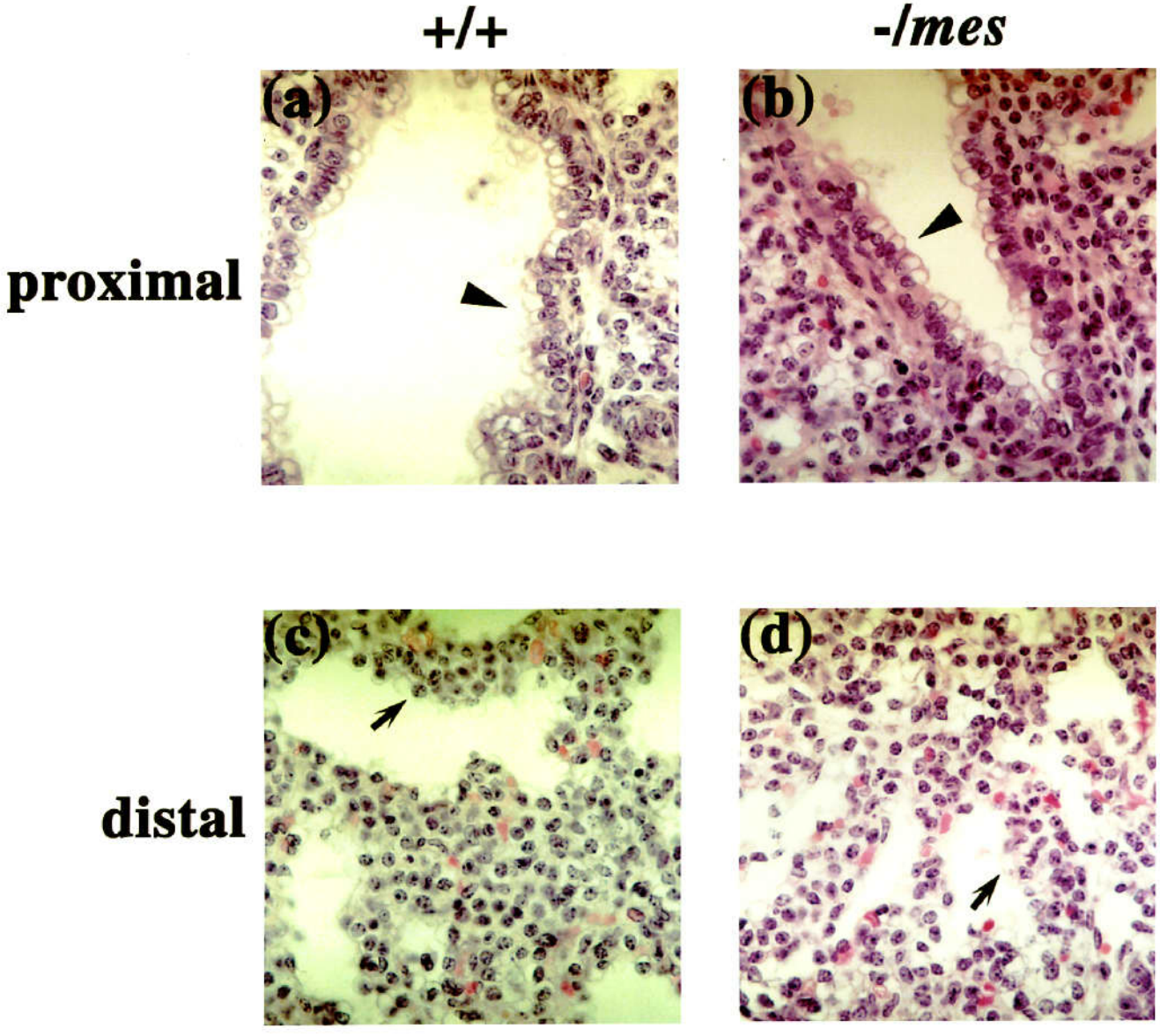

Fig. 10 Higher magnitude of the histological section of developing lung at 18.5 dpc. In $ptc^{+/+}$ (a, c), bronchiolar proximal epithelium is columnar (arrowhead), and distal epithelium is low cuboidal (arrow). In $ptc^{-/nes}$ (b, d), proximal and distal epthelium are differentiated into columnar (arrowhead) and low cuboidal (arrow) like $ptc^{+/+}$ lung. This result suggested that proximal-distal axial formation was normal in $ptc^{-/nes}$ lung.

Fig. 11

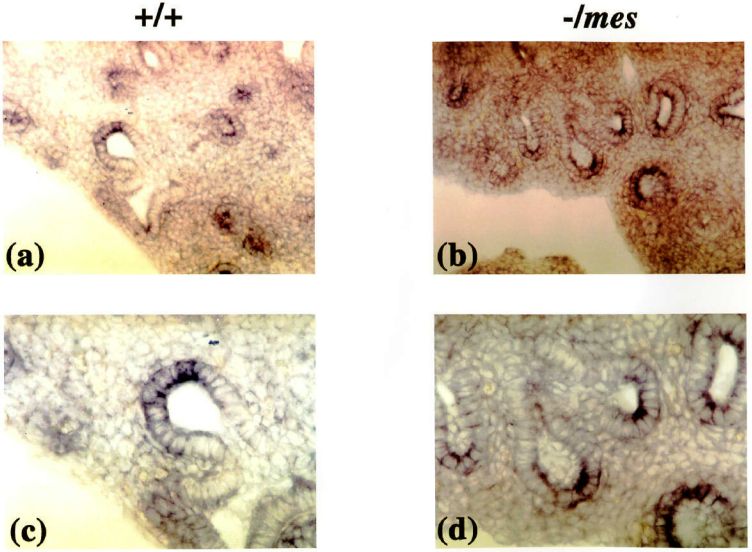

Fig. 11 *in situ* hybridization of 15.5 dpc $ptc^{+/+}$ (a, c) and $ptc^{-/mes}$ (b, d) lungs with *Bmp4* probe. (c) and (d) Higher magnitude of (a) and (b), respectively. In $ptc^{+/+}$ lung (a, c), *Bmp4* was strongly expressed at the distal tip of epithelial endoderm and weakly in mesenchyme. In $ptc^{-/mes}$ lung (b, d), *Bmp4* was expressed at the same regions as in $ptc^{+/+}$ embryo. This result suggested that proximal-distal axis was normally formed in $ptc^{-/mes}$ lung.

Fig. 12

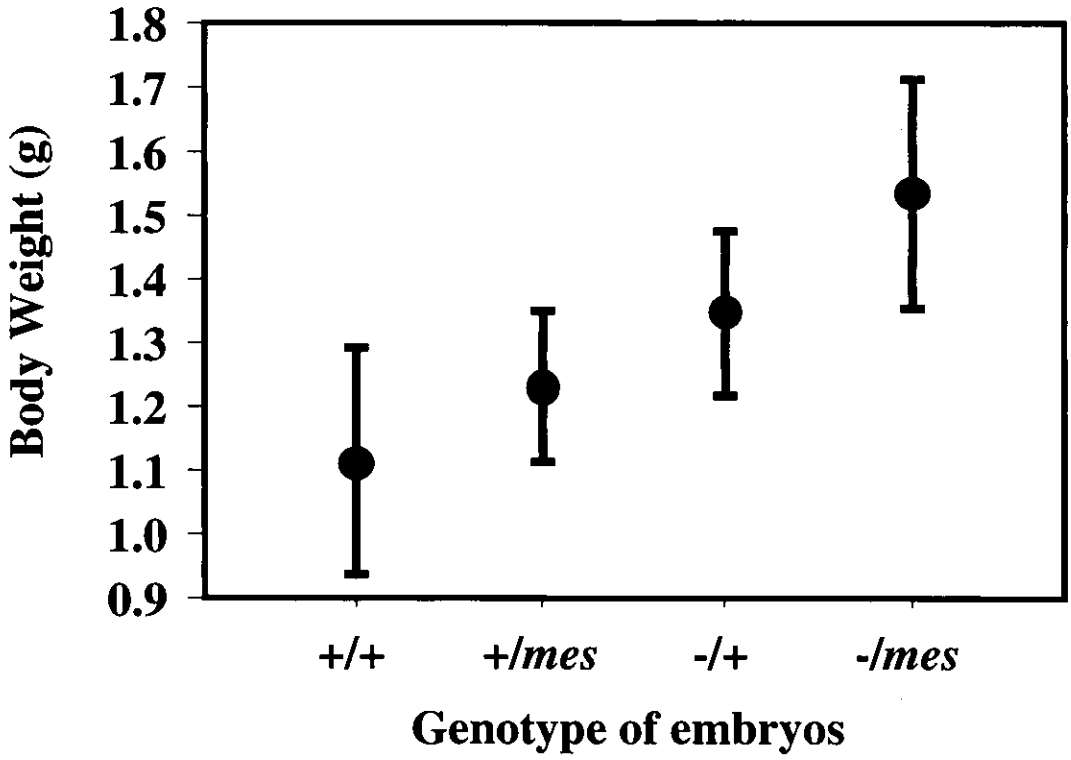
1.8
1.7
1.6
1.5
1.4
1.3
1.2
1.1
1.0
0.9
Body Weight (g)
+/+
+/mes
-/+
-/mes
Genotype of embryos

Fig. 12 Comparison of body weight of embryos with different combination of *ptc* alleles at 18.5 dpc. Average body weight of $ptc^{+/+}$, $ptc^{+/nes}$, $ptc^{-/+}$ and $ptc^{-/nes}$ was 1.115g, 1.231g, 1.384g and 1.536g, respectively, and was indicated by circles. Uppermost and lowermost lines indicate the value of ±1 S. D.

Fig. 13

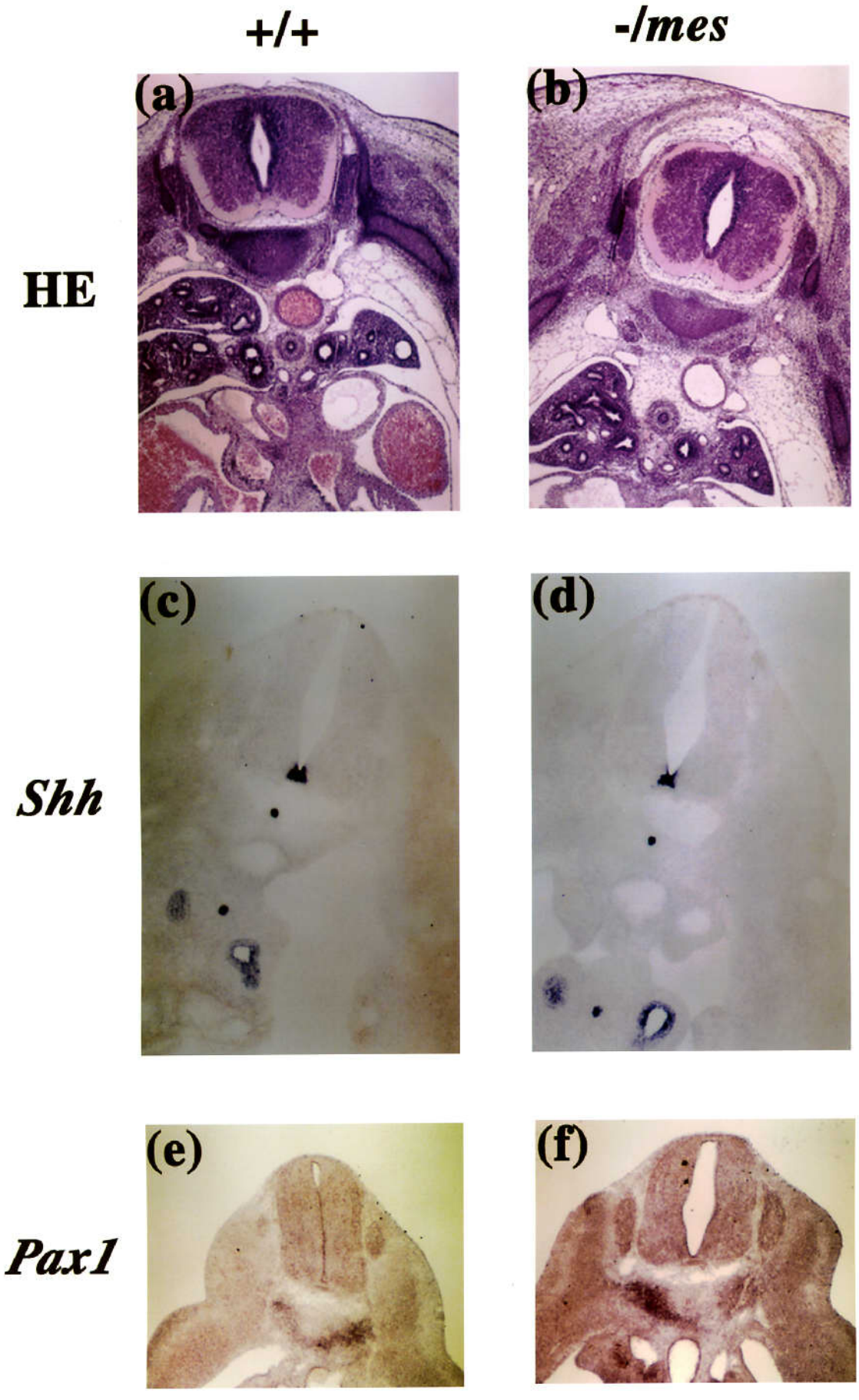

Fig. 13 Histological and *in situ* hybridization analysis of $ptc^{+/+}$ (a, c, e) and $ptc^{-/mes}$ (b, d, f) embryos. (a,b) Hematoxylin and eosin stained trunk section of 13.5 dpc embryos. Mesenchymal cells in $ptc^{-/mes}$ embryo overgrew around the neural tube, oesophagus and aorta, especially under the dorsal skin (b). (c, d) *in situ* hybridization of 11.5 dpc embryos of $ptc^{+/+}$ (c) and $ptc^{-/mes}$ (d) with *shh* probe indicated no significant difference of its expression pattern in floor plate, notochord, oesophagus and trachia. Note that as ectopic *shh* expression was not seen around the dorsal mesenchyme in $ptc^{-/mes}$ embryo (d), overgrowth of dorsal mesencymal cells likely resulted from aberrant regulation of Shh receiving cells but not from abnormal regulation of Shh secreting cells. (e, f) *in situ* hybridization of 11.5 dpc embryos with *Pax1* probe indicated that expression pattern of *Pax1* in sclerotomal cells of $ptc^{-/mes}$ (f) was same as in $ptc^{+/+}$ embryo (e). Overgrowth of mesenchymal cells did not result from overgrowth of sclerotomal cells before migrating to dorsal side. These results suggested that *ptc* acts as a negative growth regulator of mesenchymal cells independently upon Shh.

Fig. 14

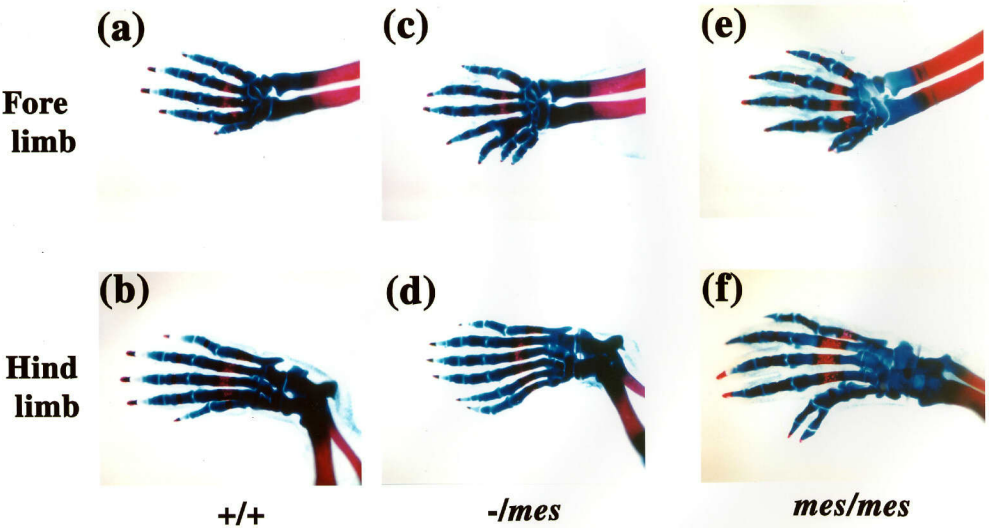

Fig. 14 Comparison of limb skeletal phenotypes. The degree of polydactylous phenotype of *ptc*$^{mes/mes}$ mice (e,f) was milder than that of *ptc*$^{-/mes}$ mice (typically 6 digits caused by bifurcation of metacarpal and matatarsal bones), but the penetrance of the phenotype was as high as 99%. All of *ptc*$^{-/mes}$ mice (c,d) to be analyzed exhibited very severe preaxial polydactyly, typically 7 digits.

Fig. 15

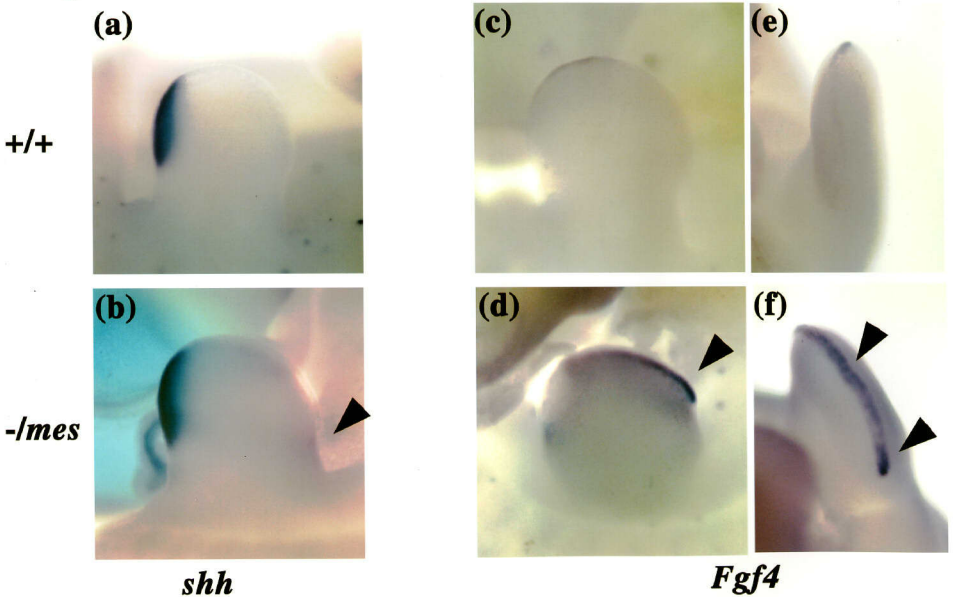

Fig. 15 Ectopic expression of *shh* and *Fgf4* in limb buds of $ptc^{-/mes}$ embryos. *in situ* hybridization of 11.5 dpc $ptc^{+/+}$ (a, c, e) and $ptc^{-/mes}$ (b, d, f) embryos was performed with cRNA of *shh* (a, b) and *Fgf4* (c-f) as probes. In $ptc^{+/+}$ embryos, *shh* was expressed only at the posterior margin of limb buds (a), whereas *shh* was expressed at the anterior margin of the limb buds in the $ptc^{-/mes}$ embryos in addition to normal expression (b, arrowhead). This ectopic expression was very weak, and I could detect it only one of two analyzed embryos but in the both hind limbs. In $ptc^{+/+}$ embryo, *Fgf4* was expressed in the posterior side of AER (c, e), whereas strong ectopic expression of *Fgf4* was observed at the anterior side of AER of all two $ptc^{-/mes}$ embryos to be analyzed (d, f). In figures, dorsal view of left hind limbs was shown (a-d). Anterior is to the right and posterior is to the left. Anterior view of right hind limbs was shown (e,f). Dorsal is to the right and ventral is to the left. Arrowheads indicate ectopic expression of *shh* and *Fgf4*.

Fig. 16

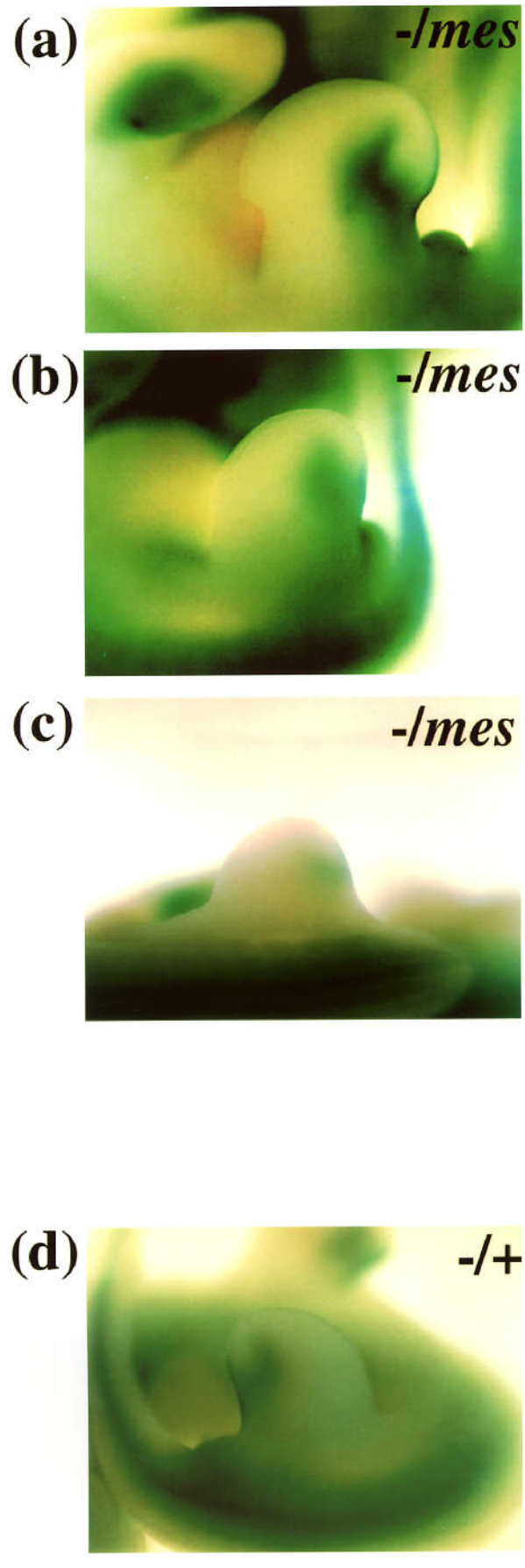

Fig. 16 *ptc-lacZ* staining of limb buds of $ptc^{-/+}$ embryo (d) and $ptc^{-/mes}$ embryos (a-c). As *lacZ* was integrated into *ptc* locus, *lacZ* staining reflected the expression of endogenous *ptc* gene. In $ptc^{-/+}$ embryo at 11.5 dpc (d), *ptc* was expressed at the posterior half of mesenchyme of the limb buds except the region in which *shh* was expressed. In $ptc^{-/mes}$ limb buds, no significant difference of *ptc* expression was observed at 11.0 dpc (c), 11.5 dpc (b) and 12.0 dpc (a). (a-c) Dorsal view of right hind limbs was shown. Anterior is to the left and posterior is to the right. (d) Dorsal view of left hind limb was shown. Anterior is to the right and posterior is to the left.